Next Chemical Engineering 2 (2026) 100055

Contents lists available at ScienceDirect

Next Chemical Engineering

journal homepage: www.sciencedirect.com/journal/next-chemical-engineering

Review article

Multiphysical analysis of the Hall and dufour effects on radiatively accelerated casson fluid flow past an inclined rotating porous plate with chemical reaction

S. Abirami [a], A. Selvaraj [a,*], A. Kavitha [b], D. Lakshmikaanth [c], G. Kuppuswami [d]

[a] Department of Mathematics, Vels Institute of Science, Technology and Advanced Studies, Chennai, 600117, India
[b] Department of Mathematics, Vel Tech High Tech Dr.Rangarajan Dr.Sakunthala Engineering College, Avadi, Chennai, India
[c] Department of Mathematics, College of Fish Nutrition & Food Technology(CFNFT), Tamilnadu Dr J.Jayalalithaa Fisheries University (TNJFU), Chennai, 600051, India
[d] Department of Mathematics, Panimalar Engineering College, Chennai, Tamil Nadu, India

ARTICLE INFO

Keywords:
Non-Newtonian casson fluid
Dufour effect
Skin-friction
Porous material
Inclined plate

ABSTRACT

The examination of non-Newtonian fluid dynamics influenced by simultaneous thermal and electromagnetic interactions is crucial for sophisticated engineering applications, including energy systems, material processing, and thermal management. This study investigates the cumulative effects of Hall current, the Dufour effect, radiation-assisted heat generation, and rotation on the unsteady flow of a Casson fluid across an inclined, exponentially accelerating, heated permeable plate. The originality of this study lies in the concurrent examination of these interrelated physical mechanisms within a rotating porous framework, which has received minimal attention in the current literature. Using the Laplace inversion method, we may write down and solve the governing equations for momentum, energy, and concentration. The findings indicate that fluid velocity increases with elevated heat generation, Hall current, and Dufour number, whereas it decreases with increasing radiation and rotational parameters. Additionally, the impacts on the skin friction coefficient, Nusselt number, and Sherwood number are measured and shown in tables and graphs.

1. Introduction

Researchers have shown significant interest in non-Newtonian Casson fluids due to their widespread application in engineering, biological, and industrial processes that involve complex flow behaviors. When such fluids pass through inclined porous surfaces, when coupled, the impacts of rotation, magnetism, reactions, and heat creation can significantly modify momentum and Heat and mass transfer properties. Incorporating Hall and Dufour-related effects provides a more realistic picture of cross-diffusion and electromagnetic interactions in electrically conducting fluids. Under exponentially accelerating conditions, velocity, temperature, and concentration profiles can be precisely evaluated through analytical investigation using the inverse Laplace transform. Optimizing heat management and fluid transport in systems like MHD generators, polymer processing, and geothermal applications requires an understanding of how radiation, rotational effects, and chemical reactions interact. The flow's mechanical and thermal performance is further measured by calculating the skin friction, Nusselt, and Sherwood values. This paper aims to provide a comprehensive understanding of the coupled influences on Casson fluid dynamics within a rotating porous medium.

M.S. Abel and N. Mahesha [1] used the method of recording and similarity conversion to study the power-law flow of fluid across a vertically extended surface. Utpal Jyoti Das [2] investigates that stronger magnetic fields and stronger Casson fluid features speed up mass transfer, while higher thermal radiation, velocity slip, and chemical reaction parameters move it down. Alam et al. [3–5] used numerical methods to investigate velocity, temperature, concentration, and other physical parameters. Radha et al. [6] use the Laplace transform method to analyze a parabolically accelerated plate under magnetic, radiative, and reactive influences. An investigation of unsteady parabolic flow that conducts electricity over an isothermal vertical plate with a first-order (chemical) reaction is carried out by Dilip Jose S. and Selvaraj A. [7]. Taking into account several variables, Jothi and Selvaraj [8,9] investigated exponential fluid movement. An analytical study explores implications with rotation spinning, magnetic fields (MHD), and thermal rays

* Corresponding author.
E-mail address: aselvaraj_ind@yahoo.co.in (A. Selvaraj).

https://doi.org/10.1016/j.nxcen.2026.100055
Received 5 February 2026; Received in revised form 5 May 2026; Accepted 5 May 2026
Available online 5 June 2026

by Karthikeyan et al. [10,11].

Kavitha et al. [12] examined analytical aspects influenced by magnetic field (MHD), rotational motion, the Dufour effect, and chemical reaction. Assume homogeneous temperature and mass diffusion. Kumar and Deka [13] discovered that coupled stratification accelerates the approach to stable states, which has applications in heat exchange design. Aruna et al. [14] emphasise that the thermal diffusion and thermal impacts are considerable for fluids with low molecular weights. Balamurugan et al. studied MHD free convection via an upward porous surface as impacted by a temperature heat source [15]. The reaction impact, radiant and MHD Casson fluid flows are examined by Manjula and Venkata Chandra Sekhar [16]. According to Dowerah, Ahmed, and Deka [17], absorption radiation raises temperature and velocity, whereas magnetic fields and chemical reactions decrease fluid velocity and concentration.

Bijjula Prabhakar Reddy et al. [18–20]'s collective studies concentrate on the dynamics of unsteady magnetohydrodynamic (MHD) convection over vertical porous and oscillating plates that are impacted by radiation, heat absorption, and chemical processes. The research uses numerical simulations to examine heat and mass transport properties while taking into account elements including Newtonian heating, slip boundary conditions, Hall current, and thermodiffusion. Their findings highlight the important interaction of radiative, magnetic, and reactive effects in regulating fluid behaviour in porous media. Prabhakar Reddy et al. [21] evaluate mainly speed, warmth and accumulation distributions by incorporating thermal radiation and using analytical techniques. The results show that chemical reactions and thermo-diffusion have a major influence.

The combined Soret and Dufour effects on mass transfer in porous media are analysed by Cheng, Ching-Yang [22–24]. The work takes into account both constant and varying boundary warmth (temperature) and accumulation (concentration) circumstances and covers vertical cylinders and inclined plates. The analyses show how temperature, concentration, and velocity distributions are affected by cross-diffusion phenomena. In engineering applications using porous media, these findings offer insights for improving heat and mass transmission. MHD flow over porous media was investigated by Chenna Kesavaiah D et al. [25,26], who looked at reactions and sort impacts on flow past inclined, vertical plates with mass transfer and heat sources. Chinmoy Rath et al. [27] show how the Dufour (Df) effect alters the speeding plate with a Hall current. The error function is the main topic of Richard B. Hetnarski's [28,29] discussion of techniques for inverting Laplace transforms. Heat source, rotation, and the Dufour effect beyond parabolically accelerated isothermal vertical plates in different porous media configurations are investigated by Lakshmikaanth D et al. [30,31]. The behaviour of Casson fluid was examined by Ameer Ahammad et al. [32], who discovered that when the Schmidt number and reaction rate grow, species concentration drops. Numerical calculations by Rajakumar et al. [33] showed that, whereas the reaction has an opposite impact, the generation of heat tends to enhance fluid velocity. Raj Kumar et al. [34] used his analytical techniques to examine the effects of magnetic fields, plate inclination, and Hall and ion-slip currents. This research provides important new information on HMT systems by demonstrating how ion-slip and Hall effects dramatically change speed.

According to M. Anil Kumar et al. [35], the concentration profile rises as the Sort number increases, while the trend is observed oppositely when the Dufour numbers increase. Rajesh V. and others [36,37] Under the impact of heat sources, collaborators study unsteady MHD flow via inclined and vertical porous plates. Variable temperature, viscous dissipation, Ohmic heating, and viscoelastic fluid behaviour are all taken into account in the assessments. The findings demonstrate how heat production and the properties of porous media greatly affect temperature, velocity, and flow stability in convective MHD systems.

Swaranalathaammal et al. [38] conducted a study examining how the interplay between radiation absorption and reactions affects the flow across an endlessly vertically sloped permeable plate. The work sheds light on how these influences affect the fluid's concentration and temperature profiles. The study by Ali et al. [39] explores the relationship between chemical processes and periodic magneto-hydrodynamics (MHD) about entropy generation across a sloped permeable plate. The work offers a statistical examination of how Dufour and Hall currents affect MHD flow in these kinds of systems. The HMT properties and heat source/sink with buoyancy effects are examined in the work by Chitra et al. [40].

Loganathan et al. [41–44] show that hybrid and Casson nanofluids under MHD, porous media, radiation, slip effects, and entropy optimisation significantly improve heat and mass transfer performance. The inclusion of nanoparticle shape factors, double diffusion models, gyrotactic microorganisms, and machine learning enhances prediction accuracy and thermal efficiency. These works highlight the importance of multi-physical and optimised modelling for advanced engineering and thermal systems. Sademaki, L. et al. [45–48] However, the findings underscored the substantial influence of radiation absorption, magnetic field intensity, and chemical reactions on velocity, temperature, concentration profiles, and degradation mechanisms in nanofluid systems. Matao et al. [49] investigated the impact of thermal radiation on fractional MHD Couette flow of Jeffrey fluid in a vertical channel, incorporating activation energy and Joule heating. Sademaki, L. et al. [50–52] elucidated the substantial effects of variable heat source/-consumption and higher-order reacting species on velocity, temperature, and concentration distributions, as reported in Multiscale and Multidisciplinary Modelling, Experiments and Design. Casson [53] studied the Casson fluid model, which characterises the non-Newtonian behaviour of pigment-oil suspensions exhibiting yield stress properties. Later, this model proved very important for studying viscoelastic flows in biofluid mechanics and engineering. Cramer et al. [54] articulated extensive principles of magnetofluid dynamics, encompassing both theoretical and practical dimensions of MHD flows. Their research constitutes a fundamental reference for the movement of electrically conductive fluids in magnetic fields. Sutton and Sherman [55] presented a technical examination of magnetohydrodynamics, focusing on its practical applications. The book talks about systems for plasma flow, electromagnetic propulsion, and MHD power generation. Greenspan [56] analysed the classical theory of rotating fluids, which explains Coriolis phenomena and geophysical fluid dynamics. Rosseland [57] came up with the Rosseland approach for radiative heat flow in an optically thick medium in 1936. Brewster [58] examined thermal radiative transport and the radiative characteristics of materials. Eckert and Drake [59] expressed the ways to study how heat and mass move in engineering systems. Nield and Bejan [60] provide a more in-depth look at convection in porous media, covering both theoretical modelling. The results show that it is easier to manage heat and mass transport in porous materials. Nonetheless, extensive study under more generalized coupled physical situations remains constrained, prompting the current investigation.

Krishnakanth and Lakshminarayana [61,62] investigated the effects of Lorentz force and induced magnetic fields on ternary hybrid and Carreau nanofluids, demonstrating significant changes in flow and temperature. In systems that are very hot, diffusion and thermal radiation are very essential. In Ref. [63], the impacts of heat diffusion and molecular motion were examined concurrently. Williamson nanofluid's non-Fourier heat conduction was discussed in Ref. [64]. Sadiya and Sucharitha [65,66] examined the flow of nanofluids in porous media under conditions of rotation, thermochemical reactions, and stratification, highlighting their impact on heat transfer. Ajithkumar et al. [67] investigated peristaltic Bingham nanofluid flow, emphasising the importance of diffusion and convective conditions.

The novelty of this research resides in the concurrent integration of coupled thermo-magnetic and reactive processes within a rotating permeable medium, alongside the analytical assessment of skin friction, Nusselt number, and Sherwood number, which has been insufficiently investigated in other works. The objective of this study is to look into how Hall current, the Dufour effect, radiation-assisted heat generation, and rotation all work together to make Casson fluid flow past a heated, inclined, exponentially accelerating, permeable plate. The study will also use the Laplace transform technique to find analytical solutions. This research work has some questions, like how do Hall current, Dufour effect, heat source, rotation and radiation collectively influence the velocity, temperature and concentration, and also, what is the impact of these parameters on engineering quantities such as skin friction, Nusselt and Sherwood numbers?

2. Mathematical formulation

In the present research, we investigate the transient flow of a viscous, incompressible, and electrically conducting fluid along a non-conductive vertical plate at $z = 0$. The x-axis runs inclined along the plate, while the z-axis extends in the normal direction into the plate. On the electrically conducting fluid, a perpendicular magnetic field B_0 is applied. Initially at the time $t^* \leq 0$ the fluid and the plate are at rest with uniform temperature T^*_∞ and Concentration C^*_∞ the plate expresses the motion $u^* = e^{wt}$. When time $t^* \geq 0$ the fluid and the plate maintain a constant temperature T^*_w and concentration C^*_w .According to these assumptions, the flow characteristics are solely determined by z and time. These circumstances serve as the foundation for the governing equations of transient flow [68–71]

i. The fluid is a viscous, incompressible, and electrically conducting non-Newtonian Casson fluid.
ii. The fluid flows past an infinite, inclined, permeable plate that is exponentially accelerating in its own plane.
iii. The plate is embedded in a rotating porous medium with constant angular velocity Ω
iv. We assume that the material properties, such as viscosity, thermal conductivity, and specific heat, are constant throughout the flow field.
v. Radiation heat flux is modelled using the Rosseland diffusion approximation.
vi. A first-order homogeneous chemical reaction is assumed in the concentration equation [72,73].
vii. Higher-order effects, such as higher-order temperature gradients or small variations in velocity across the boundary layer, are often neglected.
viii. We linearised certain nonlinear terms, particularly for the velocity or temperature profiles, to obtain analytical solutions

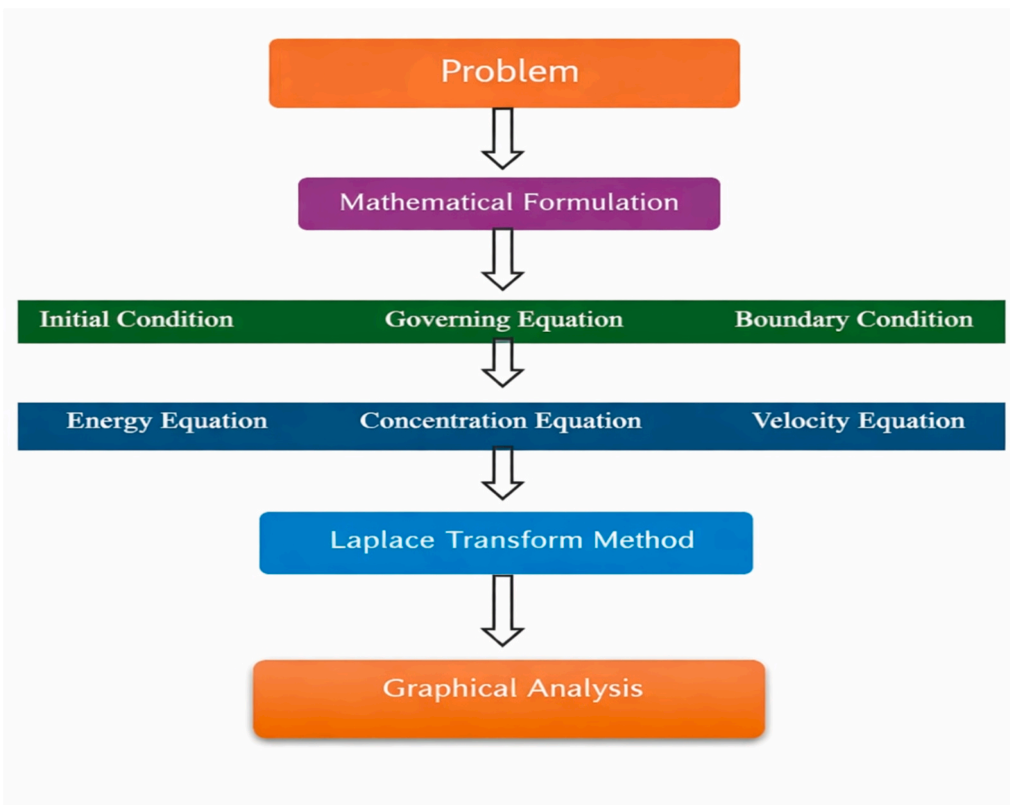

Flow chart of the Problem

$$\frac{\partial u^*}{\partial t^*} - 2\,\Omega^* v^* = \vartheta\left(1+\frac{1}{\gamma}\right)\frac{\partial^2 u^*}{\partial z^{*2}} + g\left(\beta_T\left(T^* - T^*_\infty\right)\cos\alpha + \beta_C\left(C^* - C^*_\infty\right)\right)\cos\alpha - \frac{\sigma B_0^2\left(u^* + m_1 v^*\right)}{\rho\left(1+m_1^2\right)} - \frac{\vartheta u^*}{k_1^*}\Big\} \tag{1}$$

$$\frac{\partial v^*}{\partial t^*} + 2\Omega^* u^* = \vartheta\left(1+\frac{1}{\gamma}\right)\frac{\partial^2 v^*}{\partial z^{*2}} + \frac{\sigma B_0^2\left(m_1 u^* - v^*\right)}{\rho\left(1+m_1^2\right)} - \frac{\vartheta v^*}{k_1^*} \tag{2}$$

$$\frac{\partial T^*}{\partial t^*} = \frac{k}{\rho C_p}\frac{\partial^2 T^*}{\partial z^{*2}} - \frac{1}{\rho C_p}\frac{\partial q_r}{\partial z^*} + \frac{Q_0}{\rho C_p}\left(T^* - T^*_\infty\right) + \frac{D_m K_T}{C_p C_s}\frac{\partial^2 C^*}{\partial z^{*2}} \tag{3}$$

$$\frac{\partial C^*}{\partial t^*} = \frac{1}{Sc}\frac{\partial^2 C^*}{\partial z^{*2}} - K_0\left(C^* - C^*_\infty\right) \tag{4}$$

where u is the axial and v is the transverse velocities, respectively [74, 75].

$$\left.\begin{array}{c} 0 \geq t^* : u^* = v^* = 0\,, T^* = T^*_\infty, C^* = C^*_\infty, 0 \geq z^* \\ u^* = e^{wt}, v^* = 0,\ T^* = T^*_\infty, C^* = C^*_\infty, \text{as } z^* = t^* = 0 \\ t^* > 0 : u^* \to 0, v^* \to 0, T^* \to T^*_\infty, C^* \to C^*_\infty \ \text{ as } z^* \to \infty \end{array}\right] \tag{5}$$

Using the Rosseland approximation [51], the radiative heat flux is expressed as

$$\frac{\partial q_r}{\partial z^*} = -4a^*\sigma\left(T^{*4}_\infty - T^{*4}\right) \tag{6}$$

The temperature differentials inside the flow are thought to be minimal enough that T^{*4}. They can be stated as a temperature-dependent linear function. By ignoring higher-order terms and extending the Taylor series about T^*_∞ this is achieved.

$$T^{*4} \cong 4T^{*3}_\infty T^* - 3T^{*4}_\infty \tag{7}$$

Using (6) and (7) in (3), we get

$$\frac{\partial T^*}{\partial t^*} = \frac{k}{\rho C_p}\frac{\partial^2 T^*}{\partial z^{*2}} + \frac{16\sigma T^{*3}_\infty}{3k_1\rho C_p}\frac{\partial^2 T^*}{\partial z^{*2}} + \frac{Q_0}{\rho C_p}\left(T^* - T^*_\infty\right) + \frac{D_m K_T}{C_p C_s}\frac{\partial^2 C^*}{\partial z^{*2}} \tag{8}$$

Let us assume that the non-dimensional parameters

$$\left.\begin{array}{c} u = \dfrac{u^*}{U_0}, v = \dfrac{v^*}{U_0}, z = \dfrac{z^* U_0}{\vartheta}, t = \dfrac{t^* U_0^2}{\vartheta}, \theta = \dfrac{T^* - T^*_\infty}{T^*_w - T^*_\infty}, c = \dfrac{C^* - C^*_\infty}{C^*_w - C^*_\infty} \\ G_r = \dfrac{g\beta\vartheta\left(T^*_w - T^*_\infty\right)}{U_0^3}, G_c = \dfrac{g\beta\vartheta\left(C^*_w - C^*_\infty\right)}{U_0^3}, Pr = \dfrac{\mu C_p}{k} \\ Sc = \dfrac{\vartheta}{D_m}, Df = \dfrac{D_m K_T}{C_p C_s \vartheta}\dfrac{C^*_w - C^*_\infty}{T^*_w - T^*_\infty}, k = \dfrac{\nu K_0}{U_0^2}, K_1 = \left(\dfrac{\nu^2\phi}{k_1^* U_0^2}\right), \\ M^2 = \dfrac{\sigma B_0^2\vartheta}{\rho U_0^2}, \Omega = \dfrac{\Omega^*\nu}{U_0^2}, \gamma = \dfrac{\mu_\beta}{Py}\sqrt{2\pi c} \\ R = \dfrac{4\sigma^* T^{*3}_\infty}{kk^*}, Q = \dfrac{Q_0}{\rho\, C_p \nu} \end{array}\right] \tag{9}$$

using Eqn. (6 -7) in Eqn. (3) and in Eqns. (1)–(4) we get

$$\frac{\partial U}{\partial t} = \left(1 + \frac{1}{\gamma}\right)\frac{\partial^2 U}{\partial z^2} + 2\Omega \mathrm{v} + Gr\theta(\cos\alpha) + GcC(\cos\alpha) - \frac{M^2(U + hV)}{(1 + h^2)} - \frac{U}{k_1} \tag{10}$$

$$\frac{\partial V}{\partial t} = \left(1 + \frac{1}{\gamma}\right)\frac{\partial^2 V}{\partial z^2} - 2\Omega \mathrm{u} + \frac{M^2(hU - V)}{(1 + h^2)} - \frac{V}{k_1} \tag{11}$$

$$\frac{\partial\theta}{\partial t} = \frac{1}{P_r}\frac{\partial^2\theta}{\partial z^2} - R\theta + Q\theta + Df\frac{\partial^2 C}{\partial z^2} \tag{12}$$

$$\frac{\partial C}{\partial t} = \frac{1}{S_c}\frac{\partial^2 C}{\partial z^2} - KC \tag{13}$$

using $q = U + iV$ we get

$$\frac{\partial q}{\partial t} = (G_r\theta + G_c c)\cos\alpha + \left(1 + \frac{1}{\gamma}\right)\frac{\partial^2 q}{\partial z^2} - \left(m + \frac{1}{k1}\right)q \tag{14}$$

Where $m = \frac{M^2}{(1+hi)} + 2\Omega i$

The corresponding initial and boundary conditions are

$$\left.\begin{array}{c} q = \theta = C = 0 \text{ for all } z \geq 0 \text{ and } t \leq 0 \\ q = e^{wt}, \theta = C = t \text{ for all } z = 0 \text{ and } t > 0 \\ q \to 0, \theta \to 0, C \to 0 \text{ as } z \to \infty \text{and } t > 0 \end{array}\right] \tag{15}$$

2.1. Physical significance of boundary conditions & applications

The boundary conditions tell us how the flow system works in the real world. At first, the fluid is still and has a constant temperature and concentration, which is what we call a quiescent medium. When $t > 0$, the plate starts to move in an exponential way, which makes the boundary layer unstable. The steady wall temperature and concentration make thermal and concentration gradients that cause heat and mass transfer as well as buoyancy effects. The fluid stays still far away from the plate, which makes sure that the velocity, temperature, and concentration go closer to the conditions in the room. These circumstances are relevant in engineering processes like heat exchangers, polymer extrusion, chemical reactors, and environmental flow systems.

2.2. Findings regarding fluid velocities and temperature variations

The variations of fluid velocity and temperature with governing parameters provide significant insight into the flow behaviour. An increase in parameters such as the Grashof numbers enhances buoyancy forces, leading to higher fluid velocity, whereas magnetic and rotation parameters tend to reduce velocity due to resistive forces. The Hall parameter modifies the flow structure by redistributing momentum between axial and transverse directions. Temperature profiles are strongly influenced by radiation, heat generation, and Prandtl number, where higher radiation and heat source parameters increase thermal diffusion, while larger Prandtl numbers reduce temperature thickness.

3. Solution of the problem

Solving (12), (13) and (14) using the inverse Laplace transform and applying the appropriate initial and boundary conditions

$$\theta = \theta_1 + \frac{P_r D_f S_c}{(S_c - P_r)}\theta_2 - \frac{P_r D_f S_c}{(S_c - P_r)}\theta_3 \tag{16}$$

where

$$\theta_1 = t\left[\begin{array}{l} e^{-2\eta\sqrt{P_r}\sqrt{Rt-Qt}}erfc\left(\sqrt{\eta^2 P_r} - \sqrt{(Rt - Qt)}\right) \\ +e^{2\eta\sqrt{P_r}\sqrt{Rt-Qt}}erfc\left(\sqrt{\eta^2 P_r} + \sqrt{(Rt - Qt)}\right) \end{array}\right]$$

$$-\frac{\eta\sqrt{tP_r}}{\sqrt{4(R - Q)}}\left[\begin{array}{l} e^{-2\eta\sqrt{P_r}\sqrt{Rt-Qt}}erfc\left(\sqrt{\eta^2 P_r} - \sqrt{(Rt - Qt)}\right) \\ -e^{2\eta\sqrt{P_r}\sqrt{Rt-Qt}}erfc\left(\sqrt{\eta^2 P_r} + \sqrt{(Rt - Qt)}\right) \end{array}\right]$$

$$\theta_2 = \left[\begin{array}{l} \dfrac{a + k}{2a^2}\left(\begin{array}{l} e^{at}\left[\begin{array}{l} e^{-2\eta\sqrt{P_r}\sqrt{(at+Rt-Qt)}}erfc\left(\sqrt{\eta^2 P_r} - \sqrt{(at + Rt - Qt)}\right) \\ +e^{2\eta\sqrt{P_r}\sqrt{(at+Rt-Qt)}}erfc\left(\sqrt{\eta^2 P_r} + \sqrt{(at + Rt - Qt)}\right) \end{array}\right] \\ -\left[\begin{array}{l} e^{-2\eta\sqrt{P_r}\sqrt{Rt-Qt}}erfc\left(\sqrt{\eta^2 P_r} - \sqrt{(Rt - Qt)}\right) \\ +e^{2\eta\sqrt{P_r}\sqrt{Rt-Qt}}erfc\left(\sqrt{\eta^2 P_r} + \sqrt{(Rt - Qt)}\right) \end{array}\right] \end{array}\right) \\ -\dfrac{k}{a}\left[\begin{array}{l} t\left[\begin{array}{l} e^{-2\eta\sqrt{P_r}\sqrt{Rt-Qt}}erfc\left(\sqrt{\eta^2 P_r} - \sqrt{(Rt - Qt)}\right) \\ +e^{2\eta\sqrt{P_r}\sqrt{Rt-Qt}}erfc\left(\sqrt{\eta^2 P_r} + \sqrt{(Rt - Qt)}\right) \end{array}\right] \\ -\dfrac{\sqrt{\eta^2 tP_r}}{\sqrt{4(R - Q)}}\left(\begin{array}{l} e^{-2\eta\sqrt{P_r}\sqrt{Rt-Qt}}erfc\left(\sqrt{\eta^2 P_r} - \sqrt{(Rt - Qt)}\right) \\ -e^{2\eta\sqrt{P_r}\sqrt{Rt-Qt}}erfc\left(\sqrt{\eta^2 P_r} + \sqrt{(Rt - Qt)}\right) \end{array}\right) \end{array}\right] \end{array}\right]$$

$$\theta_3 = \begin{bmatrix} \dfrac{a+k}{2a^2}\left(e^{at}\begin{bmatrix} e^{-2\eta\sqrt{S_c}\sqrt{(at+kt)}}erfc\left(\sqrt{\eta^2 Sc_r} - \sqrt{(at+kt)}\right) \\ +e^{2\eta\sqrt{S_c}\sqrt{(at+kt)}}erfc\left(\sqrt{\eta^2 Sc_r} + \sqrt{(at+kt)}\right) \end{bmatrix} - \begin{bmatrix} e^{-2\eta\sqrt{S_c}\sqrt{kt}}erfc\left(-\sqrt{kt} + \sqrt{\eta^2 Sc}\right) \\ +e^{2\eta\sqrt{S_c}\sqrt{kt}}erfc\left(\sqrt{kt} + \sqrt{\eta^2 Sc}\right) \end{bmatrix} \right) \\ -\dfrac{k}{a}\begin{bmatrix} e^{-\sqrt{4\eta^2 Sc}\sqrt{kt}}erfc\left(\sqrt{\eta^2 Sc} - \sqrt{kt}\right)\left(t - \dfrac{\eta\sqrt{tSc}}{2\sqrt{k}}\right) \\ +e^{\sqrt{4\eta^2 Sc}\sqrt{kt}}erfc\left(\sqrt{\eta^2 Sc} + \sqrt{kt}\right)\left(t + \dfrac{\eta\sqrt{tSc}}{2\sqrt{k}}\right) \end{bmatrix} \end{bmatrix}$$

$$C = \begin{bmatrix} e^{-\sqrt{4\eta^2 Sc}\sqrt{kt}}erfc\left(\sqrt{\eta^2 Sc} - \sqrt{kt}\right)\left(t - \dfrac{\eta\sqrt{tSc}}{2\sqrt{k}}\right) \\ +e^{\sqrt{4\eta^2 Sc}\sqrt{kt}}erfc\left(\sqrt{\eta^2 Sc} + \sqrt{kt}\right)\left(t + \dfrac{\eta\sqrt{tSc}}{2\sqrt{k}}\right) \end{bmatrix} \tag{17}$$

$$q_2 = \begin{bmatrix} \dfrac{e^{bt}}{2}\left(\begin{matrix} e^{-2\eta\sqrt{\frac{t}{\gamma}}\sqrt{\left(b+\frac{1}{k1}+m\right)}} erfc\left(\dfrac{\eta}{\sqrt{\gamma}} - \sqrt{bt + \dfrac{t}{k1} + mt}\right) \\ +e^{2\eta\sqrt{\frac{t}{\gamma}}\sqrt{\left(b+\frac{1}{k1}+m\right)}} erfc\left(\dfrac{\eta}{\sqrt{\gamma}} + \sqrt{bt + \dfrac{t}{k1} + mt}\right) \end{matrix} \right) \end{bmatrix}$$

$$q3 = \frac{1}{2}\left(\begin{matrix} e^{-2\eta\sqrt{\frac{t}{\gamma}}\sqrt{\left(\frac{1}{k1}+m\right)}} erfc\left(\dfrac{\eta}{\sqrt{\gamma}} - \sqrt{\dfrac{t}{k1} + mt}\right) \\ +e^{2\eta\sqrt{\frac{t}{\gamma}}\sqrt{\left(\frac{1}{k1}+m\right)}} erfc\left(\dfrac{\eta}{\sqrt{\gamma}} + \sqrt{\dfrac{t}{k1} + mt}\right) \end{matrix} \right)$$

$$q_4 = \begin{bmatrix} \dfrac{t}{2}\left(e^{-2\eta\sqrt{\frac{t}{\gamma}}\sqrt{\left(\frac{1}{k1}+m\right)}} erfc\left(\dfrac{\eta}{\sqrt{\gamma}} - \sqrt{\dfrac{t}{k1} + mt}\right) + e^{2\eta\sqrt{\frac{t}{\gamma}}\sqrt{\left(\frac{1}{k1}+m\right)}} erfc\left(\dfrac{\eta}{\sqrt{\gamma}} + \sqrt{\dfrac{t}{k1} + mt}\right) \right) \\ -\dfrac{\eta\sqrt{t}}{2\sqrt{\left(m + \dfrac{1}{k1}\right)\gamma}} \left(\begin{matrix} e^{-2\eta\sqrt{\frac{t}{\gamma}}\sqrt{\left(\frac{1}{k1}+m\right)}} erfc\left(\dfrac{\eta}{\sqrt{\gamma}} - \sqrt{\dfrac{t}{k1} + mt}\right) \\ -e^{2\eta\sqrt{\frac{t}{\gamma}}\sqrt{\left(\frac{1}{k1}+m\right)}} erfc\left(\dfrac{\eta}{\sqrt{\gamma}} + \sqrt{\dfrac{t}{k1} + mt}\right) \end{matrix} \right) \end{bmatrix}$$

$$\begin{aligned} q = {} & q_1 + \left(1 - \frac{P_r D_f S_c}{a(S_c - P_r)}k\right)(q_2 - q_3)\frac{a_1 G_r \cos\alpha}{b^2(P_r - a_1)} \\ & - \frac{a_1 G_r \cos\alpha}{b(P_r - a_1)}(q_4 + q_5)\left(1 - \frac{P_r D_f S_c}{a(S_c - P_r)}k\right) \\ & + \frac{a+k}{a^2}\frac{a_1 G_r \cos\alpha}{(P_r - a_1)}\frac{P_r D_f S_c}{(S_c - P_r)}(q_6 - q_7) \\ & - \frac{a+k}{a^2}\frac{a_1 G_r \cos\alpha}{(S_c - a_1)}\frac{P_r D_f S_c}{(S_c - P_r)}(q_8 - q_9) \\ & + (q_{10} - q_{11})\frac{a_1 Gr \cos\alpha}{(S_c - a_1)c^2}\frac{P_r D_f S_c}{(S_c - P_r)}\frac{k}{a} + (q_{12} + q_{13})\frac{a_1 G_c \cos\alpha}{(S_c - a_1)c^2} \end{aligned} \tag{18}$$

Where $q_1 = \frac{e^{wt}}{2}\begin{bmatrix} e^{-2\eta\sqrt{\frac{t}{\gamma}}\sqrt{\left(w+\frac{1}{k1}+m\right)}} erfc\left(\dfrac{\eta}{\sqrt{\gamma}} - \sqrt{wt + \dfrac{t}{k1} + mt}\right) \\ +e^{2\eta\sqrt{\frac{t}{\gamma}}\sqrt{\left(w+\frac{1}{k1}+m\right)}} erfc\left(\dfrac{\eta}{\sqrt{\gamma}} + \sqrt{wt + \dfrac{t}{k1} + mt}\right) \end{bmatrix}$

$$q_5 = \begin{bmatrix} \dfrac{e^{bt}}{2}\left(\begin{matrix} e^{-\sqrt{(b+R-Q)}2\eta\sqrt{P_r t}} erfc\left(\eta\sqrt{P_r} - \sqrt{(bt + Rt - Qt)}\right) \\ +e^{\sqrt{(b+R-Q)}2\eta\sqrt{P_r t}} erfc\left(\eta\sqrt{P_r} + \sqrt{(bt + Rt - Qt)}\right) \end{matrix} \right) \\ -\dfrac{1}{2}\left(\begin{matrix} e^{-\sqrt{(R-Q)}2\eta\sqrt{P_r t}} erfc\left(\eta\sqrt{P_r} - \sqrt{(Rt - Qt)}\right) \\ +e^{\sqrt{(R-Q)}2\eta\sqrt{P_r t}} erfc\left(\eta\sqrt{P_r} + \sqrt{(Rt - Qt)}\right) \end{matrix} \right) \\ -b\begin{bmatrix} \dfrac{t}{2}\left(\begin{matrix} e^{-\sqrt{(R-Q)}2\eta\sqrt{P_r t}} erfc\left(\eta\sqrt{P_r} - \sqrt{(Rt - Qt)}\right) \\ +e^{\sqrt{(R-Q)}2\eta\sqrt{P_r t}} erfc\left(\eta\sqrt{P_r} + \sqrt{(Rt - Qt)}\right) \end{matrix} \right) \\ -\dfrac{\eta\sqrt{tP_r}}{2\sqrt{R-Q}}\left(\begin{matrix} e^{-\sqrt{(R-Q)}2\eta\sqrt{P_r t}} erfc\left(\eta\sqrt{P_r} - \sqrt{(Rt - Qt)}\right) \\ -e^{\sqrt{(R-Q)}2\eta\sqrt{P_r t}} erfc\left(\eta\sqrt{P_r} + \sqrt{(Rt - Qt)}\right) \end{matrix} \right) \end{bmatrix} \end{bmatrix}$$

$$q_6 = \frac{1}{a-b}\left(\begin{array}{l} \frac{e^{at}}{2}\left[\begin{array}{l} e^{-2\eta\sqrt{\frac{t}{\gamma}}\sqrt{\left(a+\frac{1}{k1}+m\right)}} erfc\left(\frac{\eta}{\sqrt{\gamma}} - \sqrt{at+\frac{t}{k1}+mt}\right) \\ +e^{2\eta\sqrt{\frac{t}{\gamma}}\sqrt{\left(a+\frac{1}{k1}+m\right)}} erfc\left(\frac{\eta}{\sqrt{\gamma}} + \sqrt{at+\frac{t}{k1}+mt}\right) \end{array} \right] \\ -\frac{e^{bt}}{2}\left(\begin{array}{l} e^{-2\eta\sqrt{\frac{t}{\gamma}}\sqrt{\left(b+\frac{1}{k1}+m\right)}} erfc\left(\frac{\eta}{\sqrt{\gamma}} - \sqrt{bt+\frac{t}{k1}+mt}\right) \\ +e^{2\eta\sqrt{\frac{t}{\gamma}}\sqrt{\left(b+\frac{1}{k1}+m\right)}} erfc\left(\frac{\eta}{\sqrt{\gamma}} + \sqrt{bt+\frac{t}{k1}+mt}\right) \end{array} \right) \\ -\frac{e^{at}}{2}\left[\begin{array}{l} e^{-\sqrt{(a+R-Q)}2\eta\sqrt{P_r t}} erfc\left(\eta\sqrt{P_r} - \sqrt{(at+Rt-Qt)}\right) \\ +e^{\sqrt{(a+R-Q)}2\eta\sqrt{P_r t}} erfc\left(\eta\sqrt{P_r} + \sqrt{(at+Rt-Qt)}\right) \end{array} \right] \\ +\frac{e^{bt}}{2}\left(\begin{array}{l} e^{-\sqrt{(b+R-Q)}2\eta\sqrt{P_r t}} erfc\left(\eta\sqrt{P_r} - \sqrt{(bt+Rt-Qt)}\right) \\ +e^{\sqrt{(b+R-Q)}2\eta\sqrt{P_r t}} erfc\left(\eta\sqrt{P_r} + \sqrt{(bt+Rt-Qt)}\right) \end{array} \right) \end{array} \right)$$

$$q_7 = \frac{1}{b}\left(\begin{array}{l} \frac{e^{bt}}{2}\left(\begin{array}{l} e^{-2\eta\sqrt{\frac{t}{\gamma}}\sqrt{\left(b+\frac{1}{k1}+m\right)}} erfc\left(\frac{\eta}{\sqrt{\gamma}} - \sqrt{bt+\frac{t}{k1}+mt}\right) \\ +e^{2\eta\sqrt{\frac{t}{\gamma}}\sqrt{\left(b+\frac{1}{k1}+m\right)}} erfc\left(\frac{\eta}{\sqrt{\gamma}} + \sqrt{bt+\frac{t}{k1}+mt}\right) \end{array} \right) \\ -\frac{1}{2}\left(\begin{array}{l} e^{-2\eta\sqrt{\frac{t}{\gamma}}\sqrt{\left(\frac{1}{k1}+m\right)}} erfc\left(\frac{\eta}{\sqrt{\gamma}} - \sqrt{\frac{t}{k1}+mt}\right) \\ +e^{2\eta\sqrt{\frac{t}{\gamma}}\sqrt{\left(\frac{1}{k1}+m\right)}} erfc\left(\frac{\eta}{\sqrt{\gamma}} + \sqrt{\frac{t}{k1}+mt}\right) \end{array} \right) \\ -\frac{e^{bt}}{2}\left(\begin{array}{l} e^{-\sqrt{(b+R-Q)}2\eta\sqrt{P_r t}} erfc\left(\eta\sqrt{P_r} - \sqrt{(bt+Rt-Qt)}\right) \\ +e^{\sqrt{(b+R-Q)}2\eta\sqrt{P_r t}} erfc\left(\eta\sqrt{P_r} + \sqrt{(bt+Rt-Qt)}\right) \end{array} \right) \\ +\frac{1}{2}\left(\begin{array}{l} e^{-\sqrt{(R-Q)}2\eta\sqrt{P_r t}} erfc\left(\eta\sqrt{P_r} - \sqrt{(Rt-Qt)}\right) \\ +e^{\sqrt{(R-Q)}2\eta\sqrt{P_r t}} erfc\left(\eta\sqrt{P_r} + \sqrt{(Rt-Qt)}\right) \end{array} \right) \end{array} \right)$$

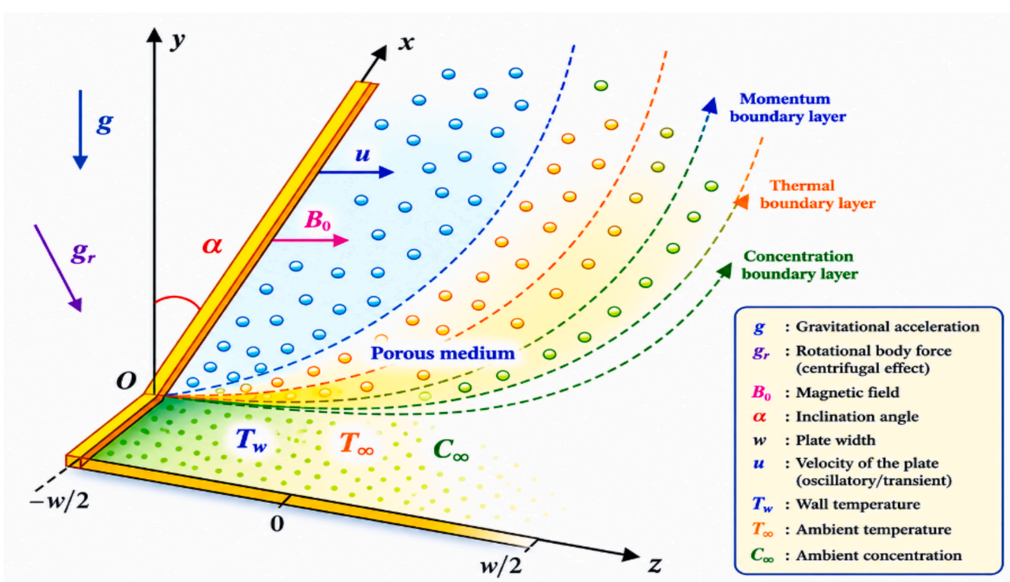

Fig. 1. Physical model of the problem.

$$q_8 = \frac{1}{2(a-c)}\left(\begin{array}{l} e^{at}\left[\begin{array}{l} e^{-2\eta\sqrt{\frac{t}{\gamma}}\sqrt{\left(a+\frac{1}{k1}+m\right)}} erfc\left(\frac{\eta}{\sqrt{\gamma}} - \sqrt{at+\frac{t}{k1}+mt}\right) \\ +e^{2\eta\sqrt{\frac{t}{\gamma}}\sqrt{\left(a+\frac{1}{k1}+m\right)}} erfc\left(\frac{\eta}{\sqrt{\gamma}} + \sqrt{at+\frac{t}{k1}+mt}\right) \end{array}\right] \\ -e^{ct}\left[\begin{array}{l} e^{-2\eta\sqrt{\frac{t}{\gamma}}\sqrt{\left(c+\frac{1}{k1}+m\right)}} erfc\left(\frac{\eta}{\sqrt{\gamma}} - \sqrt{ct+\frac{t}{k1}+mt}\right) \\ +e^{2\eta\sqrt{\frac{t}{\gamma}}\sqrt{\left(c+\frac{1}{k1}+m\right)}} erfc\left(\frac{\eta}{\sqrt{\gamma}} + \sqrt{ct+\frac{t}{k1}+mt}\right) \end{array}\right] \\ -e^{at}\left[\begin{array}{l} e^{-\sqrt{(a+k)Sct2\eta}} erfc\left(\sqrt{\eta^2(Sc)} - \sqrt{(at+(k)t)}\right) \\ +e^{\sqrt{(a+k)Sct2\eta}} erfc\left(\sqrt{\eta^2(Sc)} + \sqrt{(at+(k)t)}\right) \end{array}\right] \\ +\left[\begin{array}{l} e^{-\sqrt{k}2\eta\sqrt{Sct}} erfc\left(-\sqrt{kt} + \sqrt{\eta^2(Sc)}\right) \\ e^{\sqrt{k}2\eta\sqrt{Sct}} erfc\left(\sqrt{kt} + \sqrt{\eta^2 Sc}\right) \end{array}\right] \end{array}\right)$$

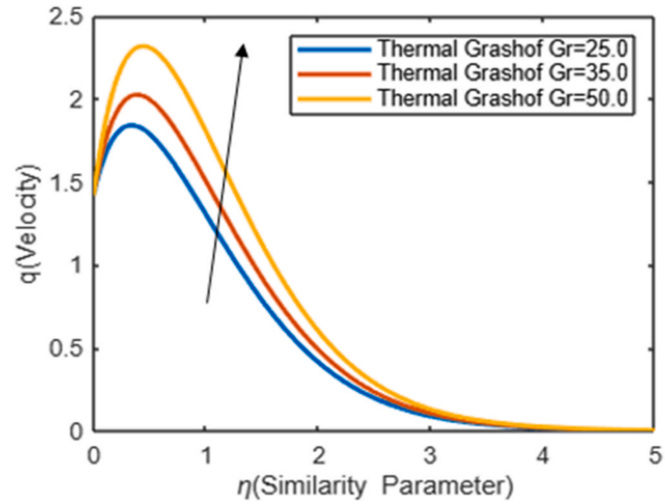

Fig. 2. Velocity(Speed) profile for Thermal Grason Gr.

$$q_9 = \frac{1}{c}\left[\begin{array}{l} \frac{e^{ct}}{2}\left[\begin{array}{l} e^{-2\eta\sqrt{\frac{t}{\gamma}}\sqrt{\left(c+\frac{1}{k1}+m\right)}} erfc\left(\frac{\eta}{\sqrt{\gamma}} - \sqrt{ct+\frac{t}{k1}+mt}\right) \\ +e^{2\eta\sqrt{\frac{t}{\gamma}}\sqrt{\left(c+\frac{1}{k1}+m\right)}} erfc\left(\frac{\eta}{\sqrt{\gamma}} + \sqrt{ct+\frac{t}{k1}+mt}\right) \end{array}\right] \\ -\frac{1}{2}\left(\begin{array}{l} e^{-2\eta\sqrt{\frac{t}{\gamma}}\sqrt{\left(\frac{1}{k1}+m\right)}} erfc\left(\frac{\eta}{\sqrt{\gamma}} - \sqrt{\frac{t}{k1}+mt}\right) \\ +e^{2\eta\sqrt{\frac{t}{\gamma}}\sqrt{\left(\frac{1}{k1}+m\right)}} erfc\left(\frac{\eta}{\sqrt{\gamma}} + \sqrt{\frac{t}{k1}+mt}\right) \end{array}\right) \\ -\frac{1}{2}\left[e^{-2\sqrt{k}\eta\sqrt{(Sc)t}} erfc\left(\sqrt{\eta^2(Sc)} - \sqrt{kt}\right) + e^{2\sqrt{k}\eta\sqrt{(Sc)t}} erfc\left(\sqrt{\eta^2(Sc)Sc} + \sqrt{kt}\right)\right] \end{array}\right]$$

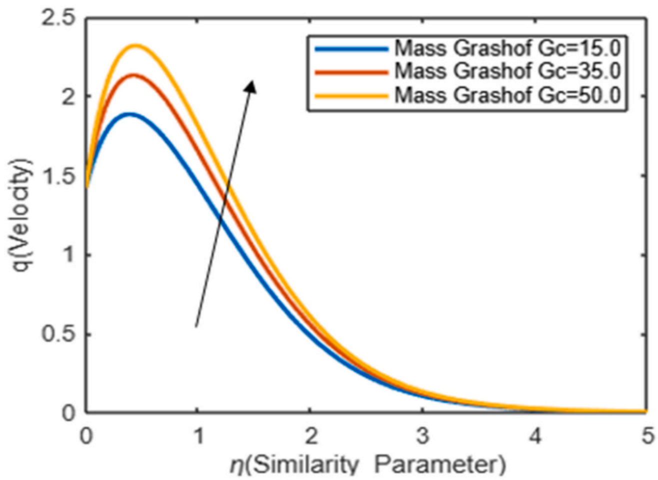

Fig. 3. Velocity(Speed) profile for Mass Graco Gc.

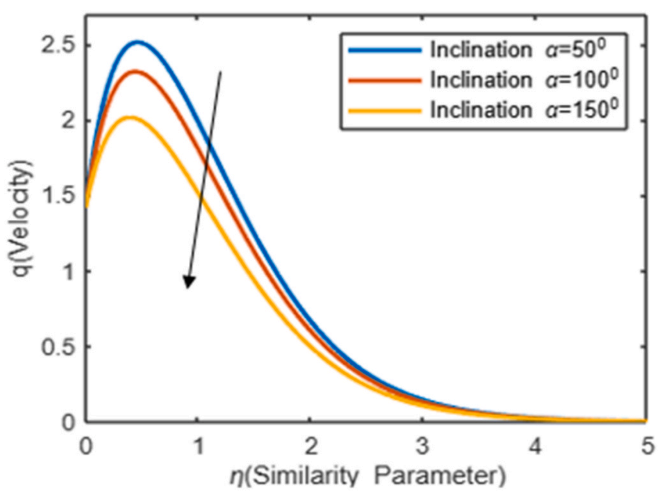

Fig. 4. Velocity(Speed) profile for distinct inclination α

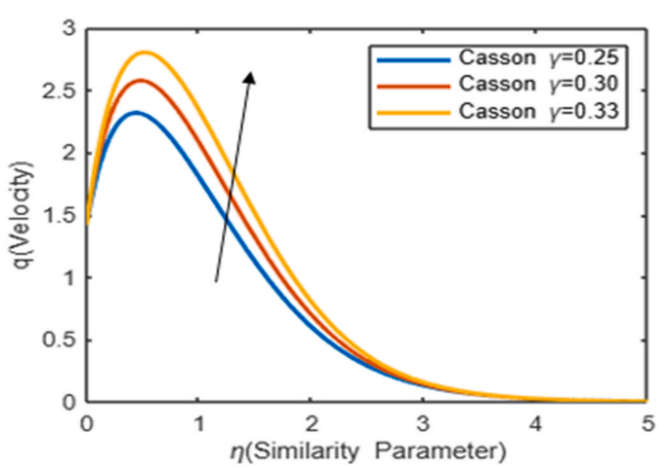

Fig. 5. Speed graph for distinct values of Casson fluid γ

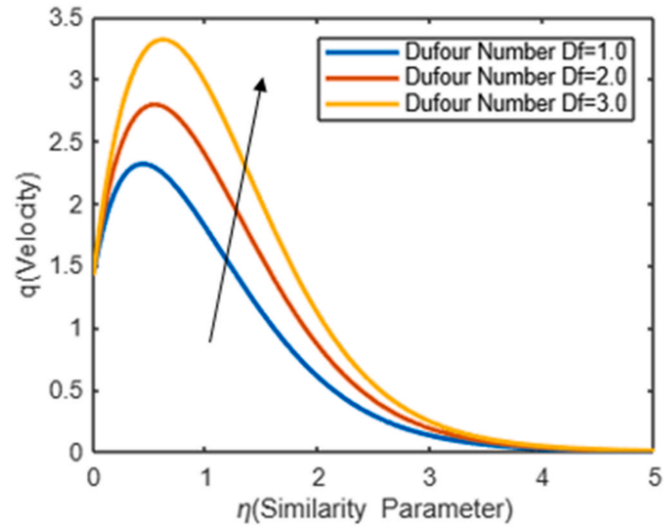

Fig. 6. Speed(Velocity) graph for Dufour Value.

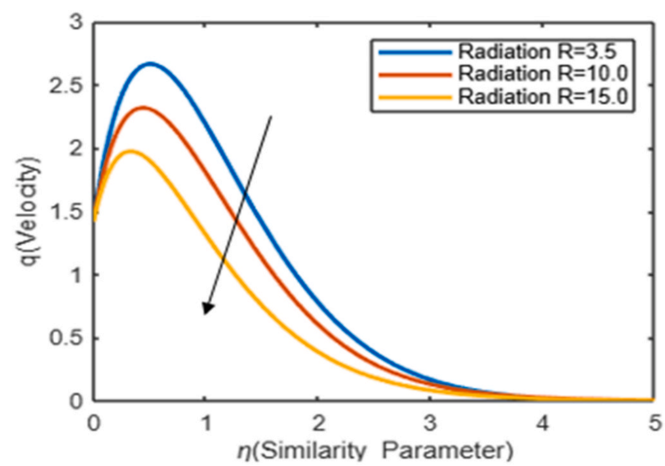

Fig. 7. Speed(Velocity) graph for various Rotational effects.

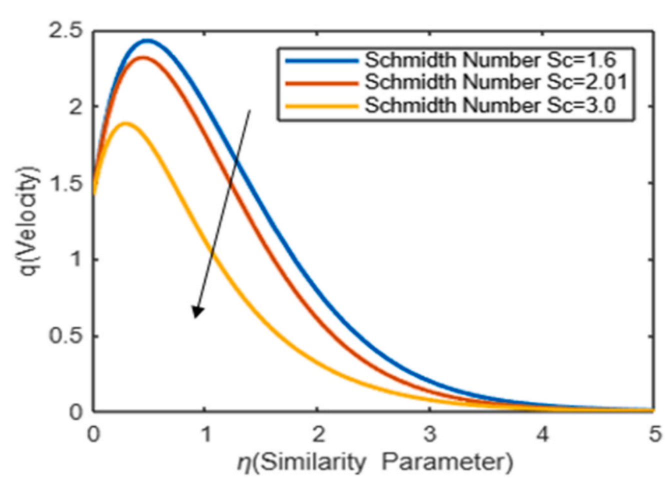

Fig. 8. Speed graph for various(different) values of Schmidth Number.

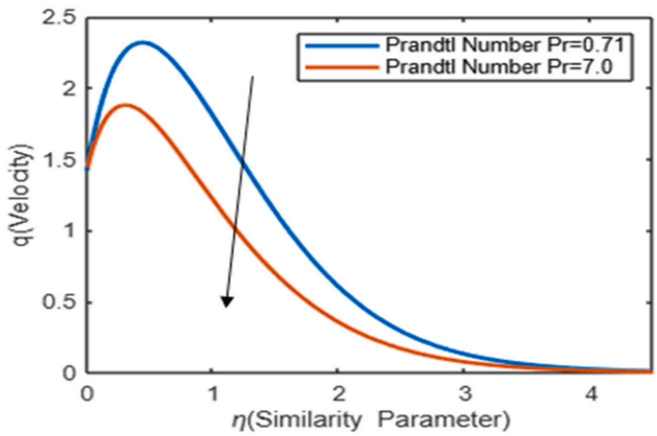

Fig. 9. Speed graph for distinct values of Prandtl Number.

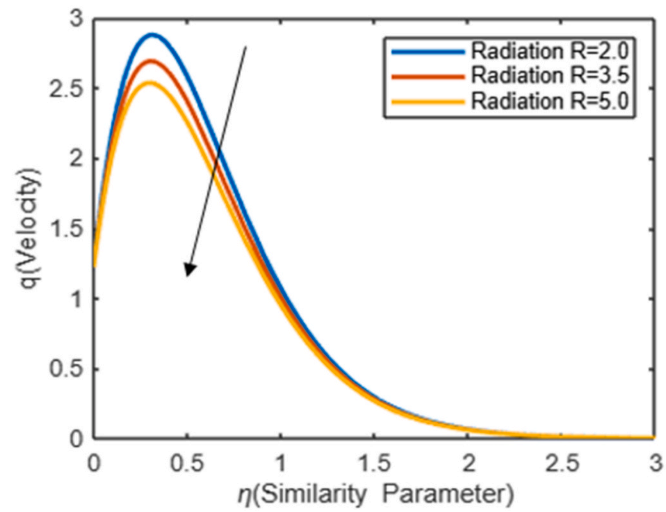

Fig. 12. Speed profile for radiation.

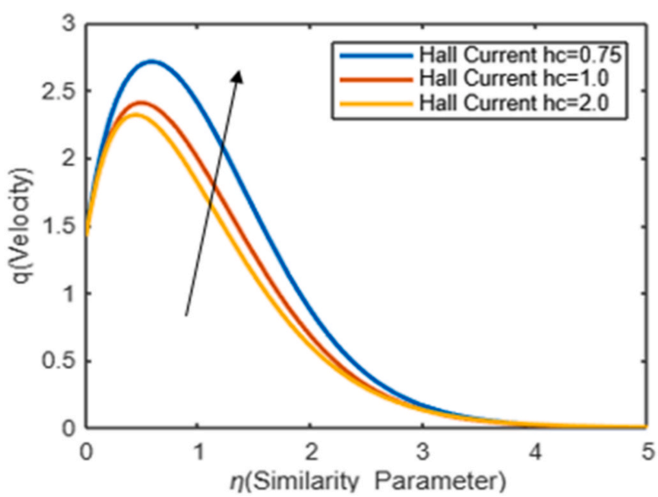

Fig. 10. Velocity(Speed) Profile for distinct values of Hall Current.

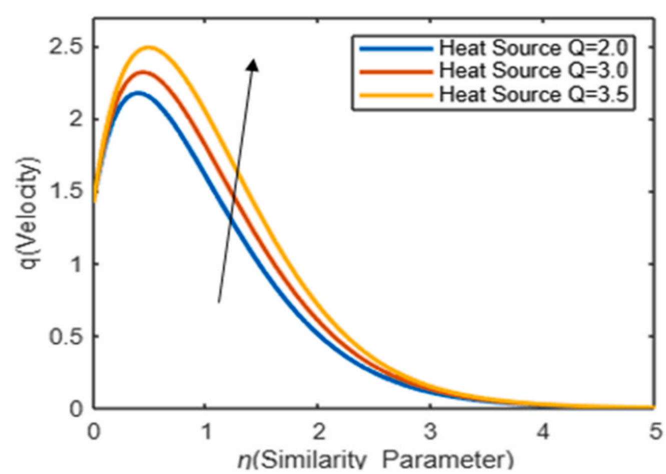

Fig. 13. Speed graph for distinct Heat Source.

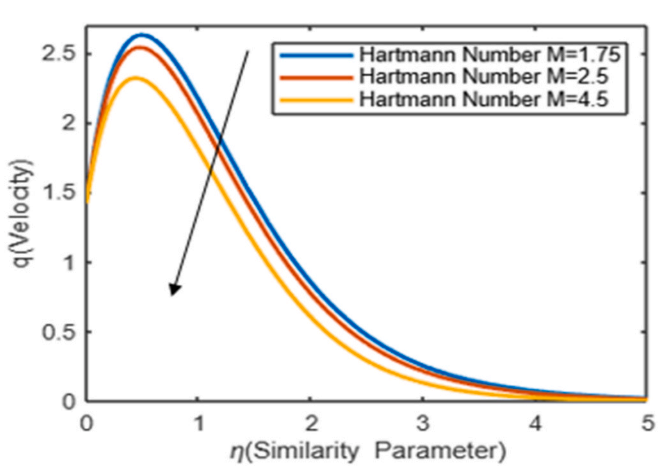

Fig. 11. Speed graph for Hartmann Number.

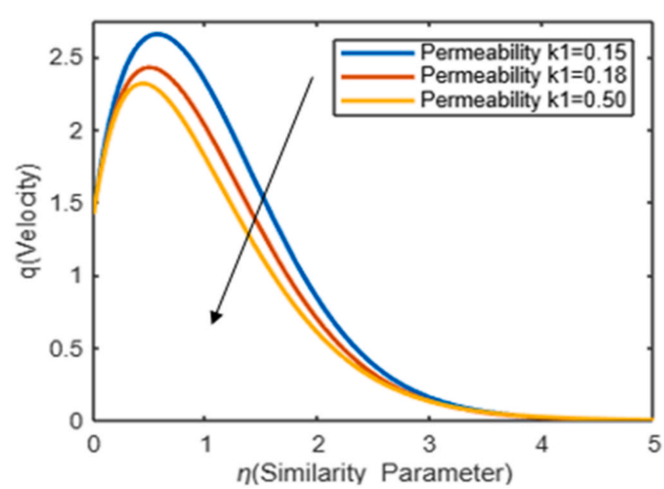

Fig. 14. Speed profile for permeability.

$$q_{10}=\left(\begin{array}{l}\dfrac{e^{ct}}{2}\left[\begin{array}{l}e^{-2\eta\sqrt{\frac{t}{\gamma}}\sqrt{\left(c+\frac{1}{k1}+m\right)}}erfc\left(\dfrac{\eta}{\sqrt{\gamma}}-\sqrt{ct+\dfrac{t}{k1}+mt}\right)\\ +e^{2\eta\sqrt{\frac{t}{\gamma}}\sqrt{\left(c+\frac{1}{k1}+m\right)}}erfc\left(\dfrac{\eta}{\sqrt{\gamma}}+\sqrt{ct+\dfrac{t}{k1}+mt}\right)\end{array}\right]\\ -\dfrac{1}{2}\left(\begin{array}{l}e^{-2\eta\sqrt{\frac{t}{\gamma}}\sqrt{\left(\frac{1}{k1}+m\right)}}erfc\left(\dfrac{\eta}{\sqrt{\gamma}}-\sqrt{\dfrac{t}{k1}+mt}\right)\\ +e^{2\eta\sqrt{\frac{t}{\gamma}}\sqrt{\left(\frac{1}{k1}+m\right)}}erfc\left(\dfrac{\eta}{\sqrt{\gamma}}+\sqrt{\dfrac{t}{k1}+mt}\right)\end{array}\right)\\ -c\left[\begin{array}{l}\dfrac{t}{2}\left(\begin{array}{l}e^{-2\eta\sqrt{\frac{t}{\gamma}}\sqrt{\left(\frac{1}{k1}+m\right)}}erfc\left(\dfrac{\eta}{\sqrt{\gamma}}-\sqrt{\dfrac{t}{k1}+mt}\right)\\ +e^{2\eta\sqrt{\frac{t}{\gamma}}\sqrt{\left(\frac{1}{k1}+m\right)}}erfc\left(\dfrac{\eta}{\sqrt{\gamma}}+\sqrt{\dfrac{t}{k1}+mt}\right)\end{array}\right)\\ -\dfrac{\eta\sqrt{t}}{2\sqrt{\left(m+\frac{1}{k1}\right)\gamma}}\left(\begin{array}{l}e^{-2\eta\sqrt{\frac{t}{\gamma}}\sqrt{\left(\frac{1}{k1}+m\right)}}erfc\left(\dfrac{\eta}{\sqrt{\gamma}}-\sqrt{\dfrac{t}{k1}+mt}\right)\\ -e^{2\eta\sqrt{\frac{t}{\gamma}}\sqrt{\left(\frac{1}{k1}+m\right)}}erfc\left(\dfrac{\eta}{\sqrt{\gamma}}+\sqrt{\dfrac{t}{k1}+mt}\right)\end{array}\right)\end{array}\right]\end{array}\right)$$

$$q_{11}=\left(\begin{array}{l}-\dfrac{1}{2}\left[e^{-\sqrt{4k}\eta\sqrt{Sct}}erfc\left(\sqrt{\eta^2Sc}-\sqrt{kt}\right)+e^{\sqrt{4k}\eta\sqrt{Sct}}erfc\left(\sqrt{\eta^2Sc}+\sqrt{kt}\right)\right]\\ +\dfrac{ce^{ct}}{2}\left(\begin{array}{l}e^{-\sqrt{(c+k)}2\eta\sqrt{Sct}}erfc\left(\sqrt{\eta^2Sc}-\sqrt{(ct+kt)}\right)\\ +e^{2\eta\sqrt{(c+k)}\sqrt{Sct}}erfc\left(\sqrt{\eta^2Sc}+\sqrt{(ct+kt)}\right)\end{array}\right)\end{array}\right)$$

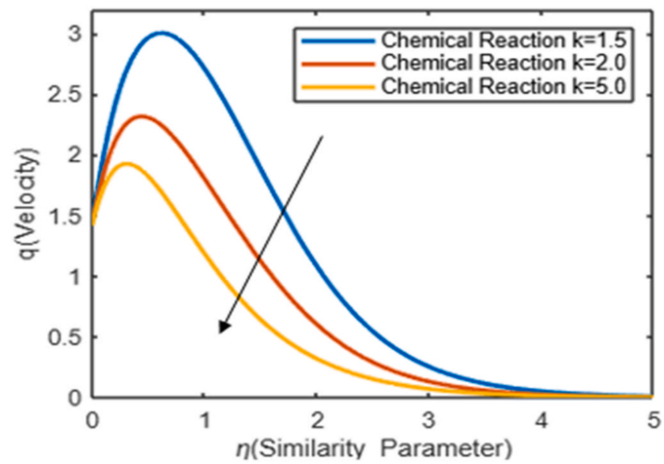

Fig. 15. Speed graph for Chemical Reaction.

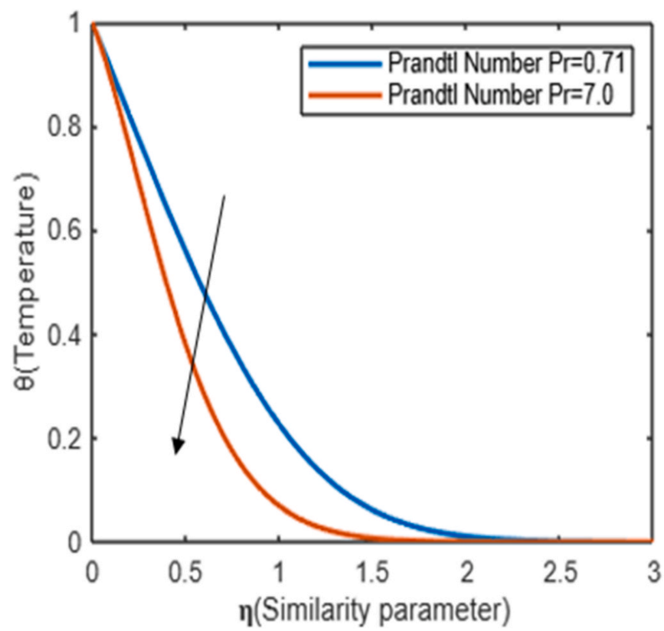

Fig. 16. Temp(Temperature) graph for Prandtl Number.

$$q_{12}=\left(\begin{array}{l}-\dfrac{1}{2}\left[e^{-\sqrt{k}(\eta)\sqrt{4(Sc)t}}erfc\left(\sqrt{\eta^2(Sc)}-\sqrt{kt}\right)+e^{\sqrt{k}\eta\sqrt{4(Sc)t}}erfc\left(\sqrt{\eta^2(Sc)}+\sqrt{kt}\right)\right]\\ +t\left[e^{-\sqrt{k}\eta\sqrt{4(Sct)}}erfc\left(\sqrt{\eta^2\ (Sc)}-\sqrt{k\,t}\right)+e^{\sqrt{k}\eta\sqrt{4(Sc)t}}erfc\left(\sqrt{\eta^2(Sc)}+\sqrt{kt}\right)\right]\\ -\dfrac{\eta\sqrt{(Sc)t}}{\sqrt{4k}}\left[e^{-\sqrt{k}(\eta)\sqrt{4Sct}}erfc\left(\sqrt{\eta^2(Sc)}-\sqrt{kt}\right)-e^{\sqrt{k}\eta\sqrt{4(Sc)t}}erfc\left(\sqrt{\eta^2(Sc)}+\sqrt{kt}\right)\right]\\ +\dfrac{ce^{ct}}{2}\left(\begin{array}{l}e^{-\sqrt{(c+k)}\eta\sqrt{4(Sc)t}}erfc\left(\sqrt{\eta^2(Sc)}-\sqrt{(ct+kt)}\right)\\ +e^{\eta\sqrt{(c+k)}\sqrt{4(Sc)t}}erfc\left(\sqrt{\eta^2(Sc)}+\sqrt{(ct+kt)}\right)\end{array}\right)\end{array}\right)$$

$$q_{13} = \left(\left(\begin{array}{l} \frac{e^{ct}}{2}\left[\begin{array}{l} e^{-2\eta\sqrt{\frac{t}{\gamma}}\sqrt{\left(c+\frac{1}{k1}+m\right)}}\, erfc\left(\frac{\eta}{\sqrt{\gamma}} - \sqrt{ct + \frac{t}{k1} + mt}\right) \\ + e^{2\eta\sqrt{\frac{t}{\gamma}}\sqrt{\left(c+\frac{1}{k1}+m\right)}}\, erfc\left(\frac{\eta}{\sqrt{\gamma}} + \sqrt{ct + \frac{t}{k1} + mt}\right) \end{array}\right] \\ -\frac{1}{2}\left(\begin{array}{l} e^{-2\eta\sqrt{\frac{t}{\gamma}}\sqrt{\left(\frac{1}{k1}+m\right)}}\, erfc\left(\frac{\eta}{\sqrt{\gamma}} - \sqrt{\frac{t}{k1} + mt}\right) \\ + e^{2\eta\sqrt{\frac{t}{\gamma}}\sqrt{\left(\frac{1}{k1}+m\right)}}\, erfc\left(\frac{\eta}{\sqrt{\gamma}} + \sqrt{\frac{t}{k1} + mt}\right) \end{array}\right) \\ -c\left[\begin{array}{l} \frac{t}{2}\left(\begin{array}{l} e^{-2\eta\sqrt{\frac{t}{\gamma}}\sqrt{\left(\frac{1}{k1}+m\right)}}\, erfc\left(\frac{\eta}{\sqrt{\gamma}} - \sqrt{\frac{t}{k1} + mt}\right) \\ + e^{2\eta\sqrt{\frac{t}{\gamma}}\sqrt{\left(\frac{1}{k1}+m\right)}}\, erfc\left(\frac{\eta}{\sqrt{\gamma}} + \sqrt{\frac{t}{k1} + mt}\right) \end{array}\right) \\ -\frac{\eta\sqrt{t}}{2\sqrt{\left(m+\frac{1}{k1}\right)\gamma}}\left(\begin{array}{l} e^{-2\eta\sqrt{\frac{t}{\gamma}}\sqrt{\left(\frac{1}{k1}+m\right)}}\, erfc\left(\frac{\eta}{\sqrt{\gamma}} - \sqrt{\frac{t}{k1} + mt}\right) \\ - e^{2\eta\sqrt{\frac{t}{\gamma}}\sqrt{\left(\frac{1}{k1}+m\right)}}\, erfc\left(\frac{\eta}{\sqrt{\gamma}} + \sqrt{\frac{t}{k1} + mt}\right) \end{array}\right) \end{array}\right] \end{array}\right)\right)$$

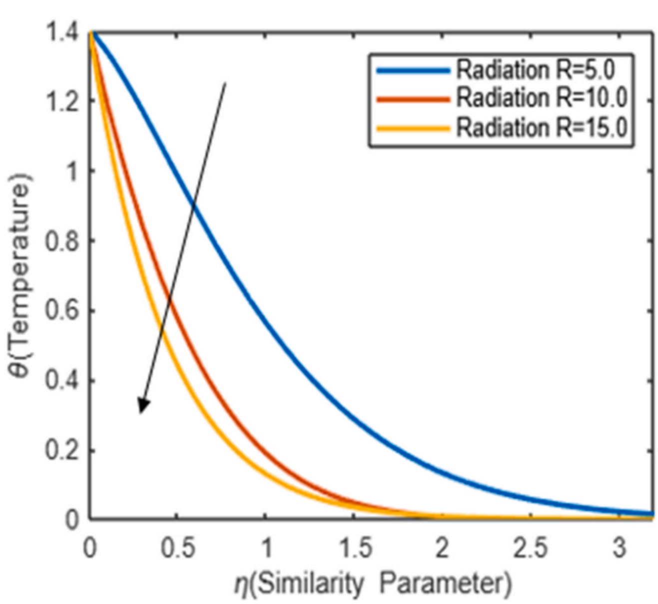

Fig. 17. Temp(Temperature) graph for radiation values.

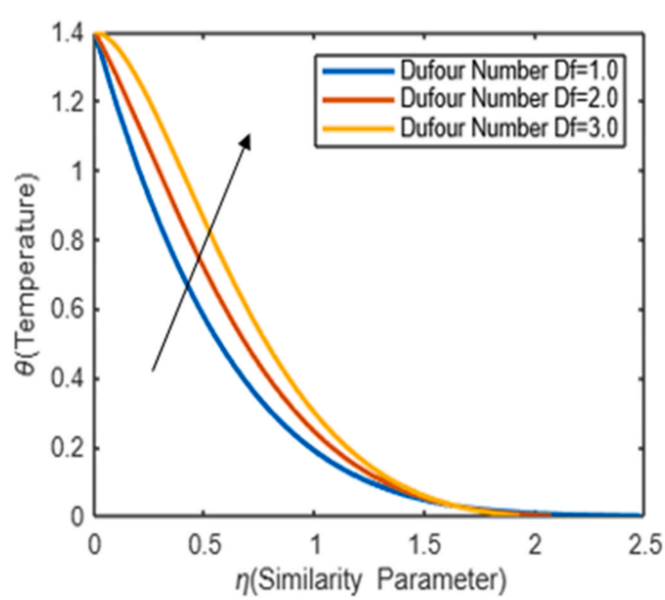

Fig. 18. Temperature graph for distinct values of Dufour Number.

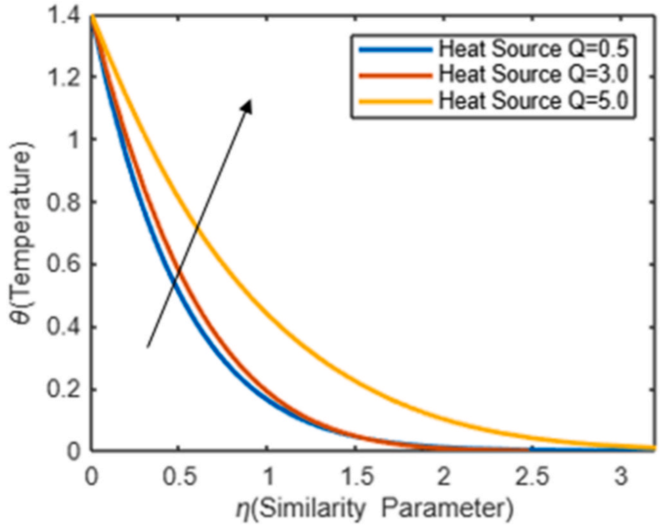

Fig. 19. Temperature graph for distinct values of Heat Source.

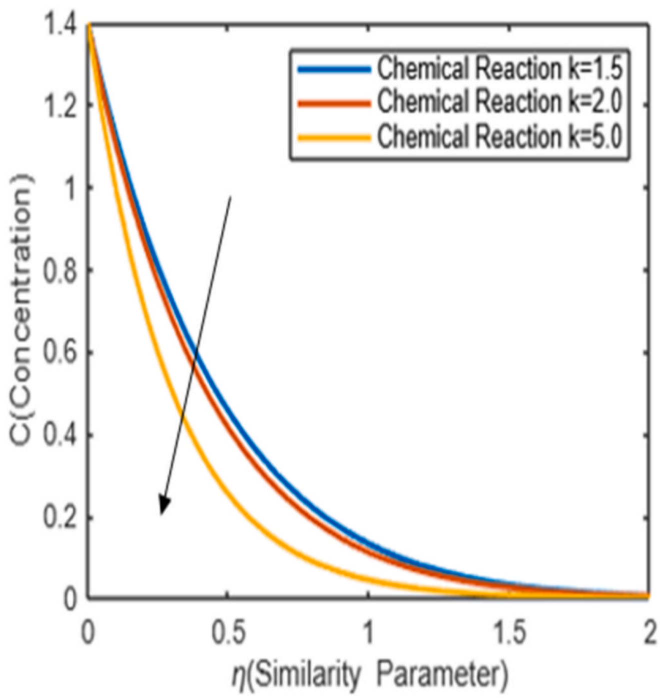

Fig. 20. Concentration graph for distinct Chemical Reaction.

$$a = \frac{-S_c k + P_r R - P_r Q}{S_c - P_r}, b = \frac{m - \gamma P_r R + \gamma P_r Q}{\gamma P_r - 1}, c = \frac{m - \gamma S_c k}{\gamma S_c - 1},$$

$$\eta = \frac{z}{2\sqrt{t}} \text{ and } a_1 = \left(1 + \frac{1}{\gamma}\right),$$

4. Results and discussion

Statistical simulations were conducted utilising numerical methods to examine the variables of q-velocity, θ-temperature, and C-concentration.

In Fig. 2, Warm Grashof Gr (25-50) raises, the velocity of the flow also rises since buoyancy dominates viscous resistance, so the fluid moves faster, hence velocity increases (see Fig. 1). Fig. 3 shows that a rise in the Accumulation Grashof Gc (15-50) increases, the flow speed

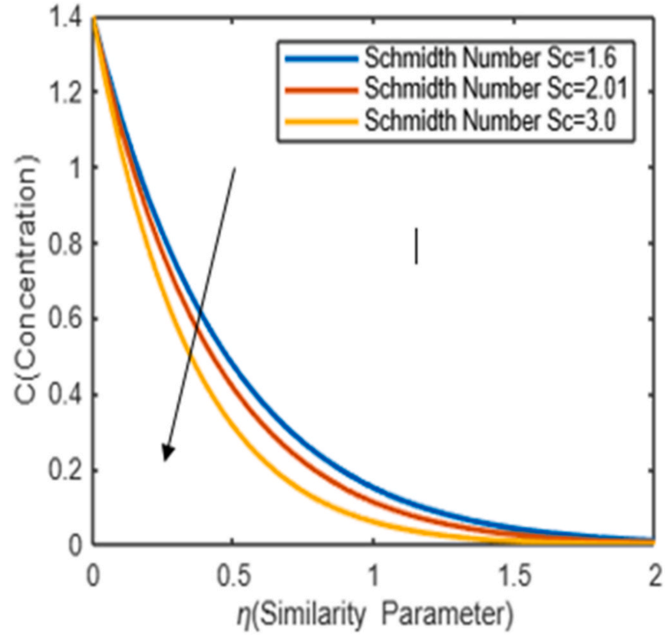

Fig. 21. Concentration graph for distinct values of Schmidt Number.

also increases. This is because a higher mass Grashof number signifies a stronger buoyancy force due to concentration differences. Fig. 4, as the inclination value α (50°-150^{0}) rises, the speed of the flow tends to increase. This is because a higher inclination angle enhances the gravitational force component acting along the plate, which accelerates the flow. Fig. 5, the Casson fluid γ (0.25 – 0.33) rises, the speed of the flow tends to rise. This is due to the enhanced flow characteristics of Casson fluids, which exhibit non-Newtonian behaviour, allowing for a higher flow velocity under certain conditions.

In Fig. 6 shows that the Dufour number Df (1.0-3.0) changes the speed of the flow, and also changes in the same direction which enhances the convective motion and thus increases the flow velocity. In Fig. 7 displays the Rotational value R(3.5-15.0) changes, and the speed of the flow changes in the opposite direction. This is because a higher rotation number introduces rotational effects, which tend to suppress the flow's velocity due to the increased centrifugal forces acting on the fluid. From Fig. 8, as the Schmidt number Sc(1.6-3.0) rises, the speed of the flow falls. This is because a higher Schmidt number indicates greater viscous diffusion compared to mass diffusion, which leads to a slower mass transfer rate and a reduction in the flow velocity. Fig. 9, as the Pr (Prandtl) number Pr (071-7.0) rises, the speed typically remains almost

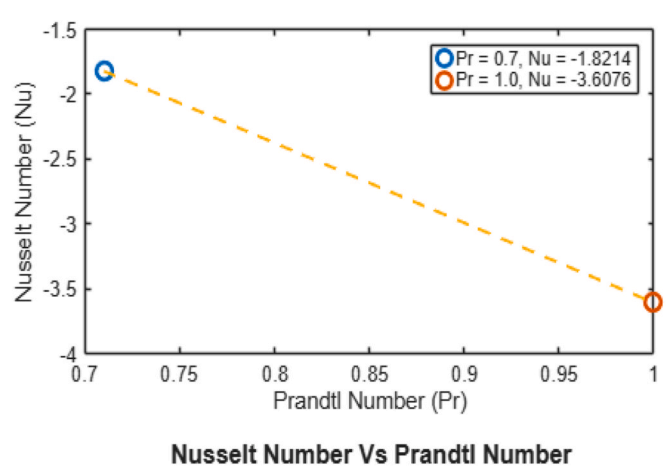

Fig. 22. Nusselt graph for distinct values of Prandtl Number Pr.

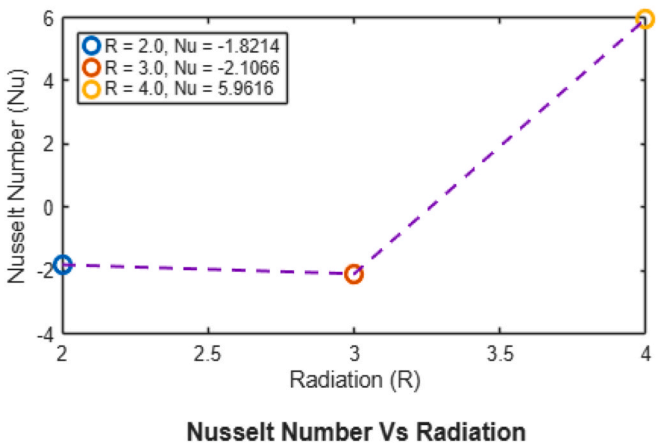

Fig. 23. Nusselt graph for distinct values of Radiation R.

unchanged. This means that heat spreads out more slowly and the thermal boundary layer gets thinner. But this change mostly impacts the temperature distribution and not the momentum field. The Prandtl number doesn't directly affect the forces that drive the momentum equation, therefore changes to it only have a little effect on the velocity field.

Fig. 10 illustrates that as the values of the Hall current hc(0.75-2.0) increase, the speed of the flow typically changes in the opposite direction. This is because the Hall current induces a magnetic force that can oppose the fluid's motion, causing a reduction in flow velocity or a reversal of its direction, depending on the flow conditions. From Fig. 11, the Hartmann number (M) (1.75-4.5) goes down, and the speed of the flow goes up. This is because a higher Hartmann number indicates a stronger magnetic field, which enhances the magnetic resistance. As the values of radiation (R) increase as Fig. 12 displays, the speed of the flow R(2.0-5.0) typically decreases. This is because increased radiation enhances heat transfer, which can lead to a reduction in the fluid's kinetic energy, thereby slowing down the flow. Fig. 13, as the values of the Thermal (Heat) source Q(2.0-3.5) rise, the speed of the flow rises. As the temperature rises, fluid density decreases due to thermal expansion, creating a stronger density difference between the hot fluid and the surrounding cooler fluid. This enhances the buoyancy force, which is the main driving force in natural convection flow. The increased buoyancy force overcomes viscous resistance more effectively, leading to an acceleration of the fluid. Therefore, the velocity of the flow increases as the thermal heat source parameter increases.

Fig. 14 shows that the Permeability k1(0.15-0.50) increases, the speed of the flow typically decreases. Fig. 15. The k reaction k(1.5-5.0) increases, and the speed of the flow typically decreases. This is because stronger chemical reactions can lead to the consumption of mass or heat, creating additional resistance in the flow and thus reducing the velocity. Fig. 16 illustrates that as the Prandtl number Pr(0.71-7.0) increases, the temperature of the fluid generally decreases. Fig. 17, the Radiation R (5.0-15.0) is high, and the temperature decreases. This is because increased radiation enhances heat loss from the fluid, leading to a cooling effect and a reduction in temperature.

As Dufour values rise, illustrated in Fig. 18, temperature typically Df (1.0-3.0) increases because the Dufour effect represents the contribution of concentration gradients to heat transfer. In other words, when there is a mass concentration difference in the fluid, it generates additional heat

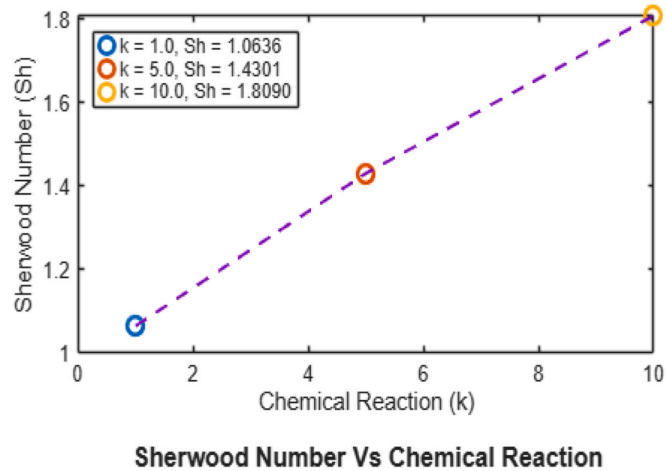

Fig. 24. Sherwood number for distinct values of Schmidt number.

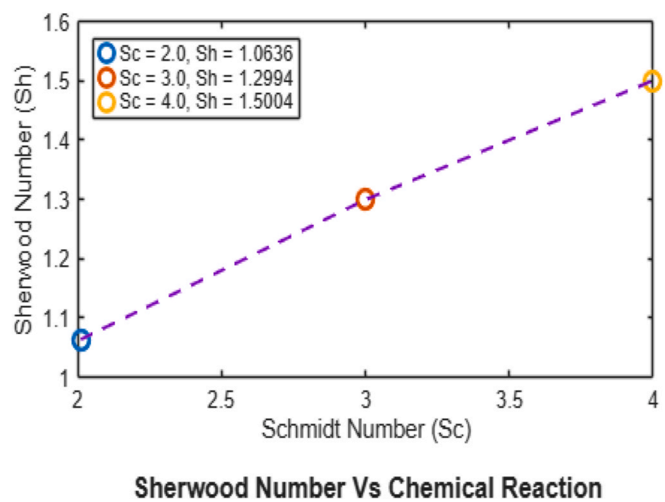

Fig. 25. Sherwood number for distinct values of Chemical Reaction.

flux. As the Dufour parameter rises, this cross-diffusion effect becomes stronger, adding extra thermal energy to the system. This supplementary heat enhances the temperature distribution within the boundary layer, resulting in an overall increase in fluid temperature. In Fig. 19, the heat (Thermal) source values Q(0.5-5.0) is high, and the temperature is also high. This is because a higher heat source provides more thermal energy to the fluid, raising its temperature. From Fig. 20, as reaction k (1.5-5.0) goes up, the concentration typically decreases. From Fig. 21, the concentration decreases as the Schmidt number(1.6-3.0) increases.

4.1. Computational analysis

4.1.1. Nusselt Number $Nu = -\left(\frac{\partial\theta}{\partial\eta}\right)_{\eta=0}$

$$Nu = -\frac{\partial\theta_1}{\partial\eta} - \frac{P_r D_f S_c}{(S_c - P_r)}\frac{\partial\theta_2}{\partial\eta} + \frac{P_r D_f S_c}{(S_c - P_r)}\frac{\partial\theta_3}{\partial\eta} \text{ at } \eta = 0$$

Where

$$\frac{\partial\theta_1}{\partial\eta} = -\left[1-erfc\left(\sqrt{(R-Q)t}\right)\right]\left[4t\sqrt{Pr}\sqrt{(R-Q)t}+\frac{\sqrt{tPr}}{\sqrt{R-Q}}\right] - \frac{2tPr}{\sqrt{\pi t}}e^{(R-Q)t}$$

$$\frac{\partial\theta_2}{\partial\eta} = \frac{a+k}{2a^2}\left(\begin{array}{l} e^{at}\left[-1+erfc\left(\sqrt{(a+R-Q)t}\right)\right]\left[4\sqrt{Pr}\sqrt{(a+R-Q)t}\right]-\frac{2\,Pr}{\sqrt{\pi t}}e^{-(a+R-Q)t} \\ +\left[1-erfc\left(\sqrt{(R-Q)t}\right)\right]\left[4\sqrt{Pr}\sqrt{(R-Q)t}\right]+\frac{2\,Pr}{\sqrt{\pi t}}e^{-(R-Q)t}-\frac{k}{a}\left(\frac{\partial\theta_1}{\partial\eta}\right)\end{array}\right)$$

$$\frac{\partial\theta_3}{\partial\eta} = \frac{a+k}{2a^2}\left(\begin{array}{l} e^{at}\left[1-erfc\left(\sqrt{(a+k)t}\right)\right]\left[-4\sqrt{Sc}\sqrt{(a+k)t}\right]-\frac{2Sc}{\sqrt{\pi t}}e^{-(a+k)t} \\ +\left[1-erfc\left(\sqrt{kt}\right)\right]\left[4\sqrt{Sc}\sqrt{kt}\right]+\frac{2Sc}{\sqrt{\pi t}}e^{-kt}-\frac{k}{a}\left(\frac{\partial C}{\partial\eta}\right)\end{array}\right)$$

The theoretical background of radiative heat transfer has been extensively discusses by Models et al[74] and Siegel et al. [75]. Rajput and Gaurav Kumar [76] studied the effects of thermal radiation and chemical reaction on MHD flow past an exponentially accelerated inclined plate, considering variable temperature, mass diffusion, and the presence of Hall current. Additionally, M.S. Elango and Lakshminarayana [77,78], which addressed the proper formulations of shear stress, heat transfer, and mass transfer characteristics. The response of the coefficient of the rate of heat transfer to changes in the physical parameters is depicted in Fig. 22 and Fig. 23 As additional energy is added to the fluid, it is found that the Nusselt number Nu rises as the heat source Q(2.0-4.0) decreases. However, by releasing heat from the system, thermal radiation R(5.0-15.0) tends to lower the Nusselt number. These findings suggest that radiative impacts and internal heat generation both have a significant impact on the pace of heat transfer. All things considered, the figure demonstrate how important Q and R are in regulating the system's thermal behaviour.

4.1.2. Sherwood number $Sh = -\left(\frac{\partial C}{\partial\eta}\right)_{\eta=0}$

$$\left(\frac{\partial C}{\partial\eta}\right)_{\eta=0} = \left(\frac{\sqrt{tSc}}{\sqrt{k}}+4t\sqrt{ktSc}\right)\left(-1+erfc\left(\sqrt{kt}\right)\right)-\frac{4t\sqrt{Sc}}{\sqrt{\pi}}e^{-kt}$$

Figs. 24 and 25 show how the Sherwood number varies with different values of the Chemical Reaction Parameter (k)(1.5-3.0) and Schmidt Number (Sc) (0.16 - 3.0). The Sherwood number's magnitude grows more negative as Sc and K rise.

4.1.3. Analysis of skin friction effects

Skin friction values, derived from the velocity (speed) field, are presented in dimensionless form as follows. $\tau = -\left(\frac{\partial q}{\partial\eta}\right)_{\eta=0}$

$$\frac{\partial q}{\partial\eta} = I_1+\left(1-\frac{P_rD_fS_c}{a(S_c-P_r)}k\right)(I_2-I_3)\frac{a_1G_r\cos\alpha}{b^2(P_r-a_1)} - \frac{a_1G_r\cos\alpha}{b(P_r-a_1)}(I_4+I_5)\left(1-\frac{P_rD_fS_c}{a(S_c-P_r)}k\right)$$
$$+\frac{a+k}{a^2}\frac{a_1G_r\cos\alpha}{(P_r-a_1)}\frac{P_rD_fS_c}{(S_c-P_r)}(I_6-I_7)-\frac{a+k}{a^2}\frac{a_1G_r\cos\alpha}{(S_c-a_1)}\frac{P_rD_fS_c}{(S_c-P_r)}(I_8-I_9)$$
$$+(I_{10}-I_{11})\frac{a_1Gr\cos\alpha}{(S_c-a_1)c^2}\frac{P_rD_fS_c}{(S_c-P_r)}\frac{k}{a}+(I_{12}+I_{13})\frac{a_1G_c\cos\alpha}{(S_c-a_1)c^2}$$

$$I_1 = \frac{e^{wt}}{2}\left[\left(\frac{-2}{\sqrt{\gamma\pi t}}\right)e^{-\left(wt+\frac{t}{k_1}+mt\right)}+4\left(-1+erfc\left(\sqrt{wt+\frac{t}{k_1}+mt}\right)\right)\left(\sqrt{\frac{t}{\gamma}}\sqrt{w+\frac{1}{k_1}+m}\right)\right]$$

$$I_2 = \frac{e^{bt}}{2}\left[\left(\frac{-2}{\sqrt{\gamma\pi t}}\right)e^{-\left(bt+\frac{t}{k_1}+mt\right)}+4\left(-1+erfc\left(\sqrt{bt+\frac{t}{k_1}+mt}\right)\right)\left(\sqrt{\frac{t}{\gamma}}\sqrt{b+\frac{1}{k_1}+m}\right)\right]$$

$$I_3 = \frac{1}{2}\left[\left(\frac{-2}{\sqrt{\gamma\pi t}}\right)e^{-\left(\frac{t}{k_1}+mt\right)}+4\left(-1+erfc\left(\sqrt{\frac{t}{k_1}+mt}\right)\right)\left(\sqrt{\frac{t}{\gamma}}\sqrt{\frac{1}{k_1}+m}\right)\right]$$

$$I_4 = I_3-\sqrt{\frac{t}{\gamma\left(\frac{1}{k_1}+m\right)}}\left(1-erfc\left(\sqrt{\frac{t}{k_1}+mt}\right)\right)$$

$$I_5 = \frac{e^{bt}}{2}\left[\left(\frac{-2\sqrt{Pr}}{\sqrt{\pi t}}\right)e^{-(bt+Rt-Qt)}+4\left(-1+erfc\left(\sqrt{bt+Rt-Qt}\right)\right)\left(\sqrt{tPr}\sqrt{b+R-Q}\right)\right]$$
$$-\frac{1}{2}(1+bt)\left(\frac{-2\sqrt{Pr}}{\sqrt{\pi t}}\right)e^{-(Rt-Qt)}+4\left(-1+erfc\left(\sqrt{Rt-Qt}\right)\right)\left(\sqrt{tPr}\sqrt{R-Q}\right)$$

$$+\frac{b\sqrt{tPr}}{\sqrt{R-Q}}\left(1-erfc\left(\sqrt{Rt-Qt}\right)\right)$$

$$I_6=\frac{1}{a-b}\left[\begin{array}{l}\frac{e^{at}}{2}\left[\left(\frac{-2}{\sqrt{\gamma\pi t}}\right)e^{-\left(at+\frac{t}{k_1}+mt\right)}-4\left(1-erfc\left(\sqrt{at+\frac{t}{k_1}+mt}\right)\right)\left(\sqrt{\frac{t}{\gamma}}\sqrt{a+\frac{1}{k_1}+m}\right)\right]\\ -\frac{e^{bt}}{2}\left[\left(\frac{-2}{\sqrt{\gamma\pi t}}\right)e^{-\left(bt+\frac{t}{k_1}+mt\right)}-4\left(1-erfc\left(\sqrt{bt+\frac{t}{k_1}+mt}\right)\right)\left(\sqrt{\frac{t}{\gamma}}\sqrt{b+\frac{1}{k_1}+m}\right)\right]\\ -\frac{e^{at}}{2}\left[\left(\frac{-2\sqrt{Pr}}{\sqrt{\pi t}}\right)e^{-(at+Rt-Qt)}-4\left(1-erfc\left(\sqrt{at+Rt-Qt}\right)\right)\left(\sqrt{\frac{t}{\gamma}}\sqrt{a+R-Q}\right)\right]\\ +\frac{e^{bt}}{2}\left[\left(\frac{-2\sqrt{Pr}}{\sqrt{\pi t}}\right)e^{-(bt+Rt-Qt)}-4\left(1-erfc\left(\sqrt{bt+Rt-Qt}\right)\right)\left(\sqrt{\frac{t}{\gamma}}\sqrt{b+R-Q}\right)\right]\end{array}\right]$$

$$I_7=\frac{1}{b}\left[\begin{array}{l}\frac{e^{bt}}{2}\left[\left(\frac{-2}{\sqrt{\gamma\pi t}}\right)e^{-\left(bt+\frac{t}{k_1}+mt\right)}-4\left(1-erf\,c\left(\sqrt{bt+\frac{t}{k_1}+mt}\right)\right)\left(\sqrt{\frac{t}{\gamma}}\sqrt{b+\frac{1}{k_1}+m}\right)\right]\\ -\frac{1}{2}\left[\left(\frac{-2}{\sqrt{\gamma\pi t}}\right)e^{-\left(\frac{t}{k_1}+mt\right)}-4\left(1-erfc\left(\sqrt{\frac{t}{k_1}+mt}\right)\right)\left(\sqrt{\frac{t}{\gamma}}\sqrt{\frac{1}{k_1}+m}\right)\right]\\ -\frac{e^{bt}}{2}\left[\left(\frac{-2\sqrt{Pr}}{\sqrt{\pi t}}\right)e^{-(bt+Rt-Qt)}-4\left(1-erfc\left(\sqrt{bt+Rt-Qt}\right)\right)\left(\sqrt{tPr}\sqrt{b+R-Q}\right)\right]\\ +\frac{1}{2}\left[\left(\frac{-2\sqrt{Pr}}{\sqrt{\pi t}}\right)e^{-(Rt-Qt)}-4\left(1-erfc\left(\sqrt{Rt-Qt}\right)\right)\left(\sqrt{tPr}\sqrt{R-Q}\right)\right]\end{array}\right]$$

$$I_8=\frac{1}{a-c}\left[\begin{array}{l}\frac{e^{at}}{2}\left[\left(\frac{-2}{\sqrt{\gamma\pi t}}\right)e^{-\left(at+\frac{t}{k_1}+mt\right)}-4\left(1-erfc\left(\sqrt{at+\frac{t}{k_1}+mt}\right)\right)\left(\sqrt{\frac{t}{\gamma}}\sqrt{a+\frac{1}{k_1}+m}\right)\right]\\ -\frac{e^{ct}}{2}\left[\left(\frac{-2}{\sqrt{\gamma\pi t}}\right)e^{-\left(ct+\frac{t}{k_1}+mt\right)}-4\left(1-erfc\left(\sqrt{ct+\frac{t}{k_1}+mt}\right)\right)\left(\sqrt{\frac{t}{\gamma}}\sqrt{c+\frac{1}{k_1}+m}\right)\right]\\ -\frac{e^{at}}{2}\left[\left(\frac{-2\sqrt{Sc}}{\sqrt{\pi t}}\right)e^{-(at+kt)}-4\left(1-erfc\left(\sqrt{at+kt}\right)\right)\left(\sqrt{tSc}\sqrt{a+k}\right)\right]\\ +\frac{1}{2}\left[\left(\frac{-2\sqrt{Sc}}{\sqrt{\pi t}}\right)e^{-(kt)}-4\left(1-erfc\left(\sqrt{kt}\right)\right)\left(\sqrt{tSc}\sqrt{k}\right)\right]\end{array}\right]$$

$$I_9=\frac{1}{c}\begin{bmatrix}\frac{e^{ct}}{2}\left[\left(\frac{-2}{\sqrt{\gamma\pi t}}\right)e^{-\left(ct+\frac{t}{k_1}+mt\right)}-4\left(1-erfc\left(\sqrt{ct+\frac{t}{k_1}+mt}\right)\right)\left(\sqrt{\frac{t}{\gamma}}\sqrt{c+\frac{1}{k_1}+m}\right)\right]\\ -\frac{1}{2}\left[\left(\frac{-2}{\sqrt{\gamma\pi t}}\right)e^{-\left(\frac{t}{k_1}+mt\right)}-4\left(1-erfc\left(\sqrt{\frac{t}{k_1}+mt}\right)\right)\left(\sqrt{\frac{t}{\gamma}}\sqrt{\frac{1}{k_1}+m}\right)\right]\\ -\frac{1}{2}\left[\left(\frac{-2\sqrt{Sc}}{\sqrt{\pi t}}\right)e^{-(kt)}-4\left(1-erfc\left(\sqrt{kt}\right)\right)\left(\sqrt{tSc}\sqrt{k}\right)\right]\end{bmatrix}$$

$$I_{10}=\begin{bmatrix}\frac{e^{ct}}{2}\left[\left(\frac{-2}{\sqrt{\gamma\pi t}}\right)e^{-\left(ct+\frac{t}{k_1}+mt\right)}-4\left(1-erfc\left(\sqrt{ct+\frac{t}{k_1}+mt}\right)\right)\left(\sqrt{\frac{t}{\gamma}}\sqrt{c+\frac{1}{k_1}+m}\right)\right]\\ -\frac{1}{2}(1+ct)\left[\left(\frac{-2}{\sqrt{\gamma\pi t}}\right)e^{-\left(\frac{t}{k_1}+mt\right)}-4\left(1-erfc\left(\sqrt{\frac{t}{k_1}+mt}\right)\right)\left(\sqrt{\frac{t}{\gamma}}\sqrt{\frac{1}{k_1}+m}\right)\right]\\ +c\sqrt{\frac{t}{\gamma\left(\frac{1}{k_1}+m\right)}}\left(1-erfc\left(\sqrt{\frac{t}{k_1}+mt}\right)\right)\end{bmatrix}$$

$$I_{11}=-\frac{1}{2}\left[\left(\frac{-2\sqrt{Sc}}{\sqrt{\pi t}}\right)e^{-(kt)}-4\left(1-erfc\left(\sqrt{kt}\right)\right)\left(\sqrt{tSc}\sqrt{k}\right)\right]$$
$$+\frac{ce^{ct}}{2}\left[\left(\frac{-2\sqrt{Sc}}{\sqrt{\pi t}}\right)e^{-(c+k)t}-4\left(1-erfc\left(\sqrt{(c+k)t}\right)\right)\left(\sqrt{tSc}\sqrt{c+k}\right)\right]$$

Skin friction rises as the Dufour number (Df) increases, as seen in Fig. 26. By intensifying the buoyancy-driven motion close to the wall and raising the temperature gradient, the Dufour effect improves energy–mass coupling in the flow. Higher skin friction results from an increase in the velocity gradient at the surface. As a result, momentum transmission within the boundary layer is greatly enhanced by the

$$I_{12}=\left(t-\frac{1}{2}\right)\left[\left(\frac{-2\sqrt{Sc}}{\sqrt{\pi t}}\right)e^{-kt}-4\left(1-erfc\left(\sqrt{kt}\right)\right)\left(\sqrt{tSc}\sqrt{k}\right)\right]-\left(1-erfc\left(\sqrt{kt}\right)\right)\left(\frac{\sqrt{tSc}}{\sqrt{k}}\right)$$
$$+\frac{ce^{ct}}{2}\left[\left(\frac{-2\sqrt{Sc}}{\sqrt{\pi t}}\right)e^{-(c+k)t}-4\left(1-erfc\left(\sqrt{(c+k)t}\right)\right)\left(\sqrt{tSc}\sqrt{c+k}\right)\right]$$

$$I_{13}=\begin{bmatrix}\frac{e^{ct}}{2}\left[\left(\frac{-2}{\sqrt{\gamma\pi t}}\right)e^{-\left(ct+\frac{t}{k_1}+mt\right)}-4\left(1-erfc\left(\sqrt{ct+\frac{t}{k_1}+mt}\right)\right)\left(\sqrt{\frac{t}{\gamma}}\sqrt{c+\frac{1}{k_1}+m}\right)\right]\\ -\frac{1}{2}(1+ct)\left[\left(\frac{-2}{\sqrt{\gamma\pi t}}\right)e^{-\left(\frac{t}{k_1}+mt\right)}-4\left(1-erfc\left(\sqrt{\frac{t}{k_1}+mt}\right)\right)\left(\sqrt{\frac{t}{\gamma}}\sqrt{\frac{1}{k_1}+m}\right)\right]\\ +c\sqrt{\frac{t}{\gamma\left(\frac{1}{k_1}+m\right)}}\left(1-erfc\left(\sqrt{\frac{t}{k_1}+mt}\right)\right)\end{bmatrix}$$

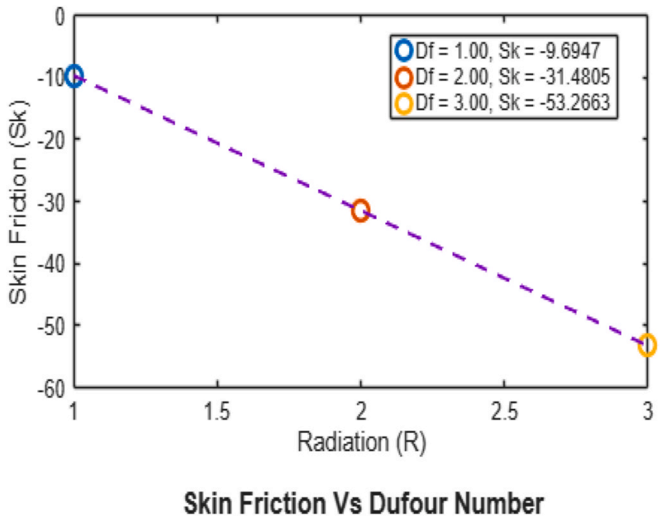

Fig. 26. Skin friction graph for distinct values of Dufour Number.

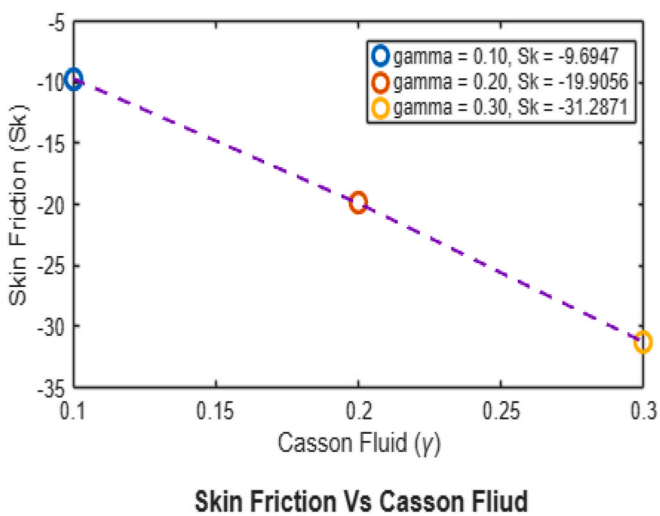

Fig. 27. Skin friction graph for distinct values of Casson fluid parameter.

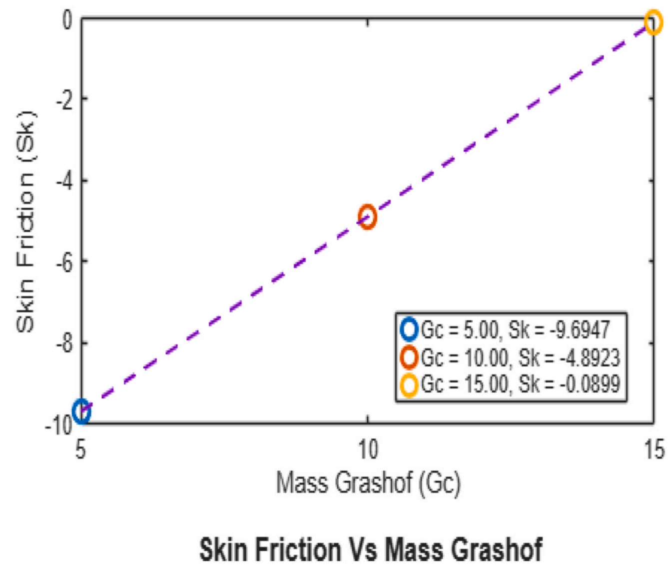

Fig. 28. Skin friction graph for distinct values of Mass Grashof.

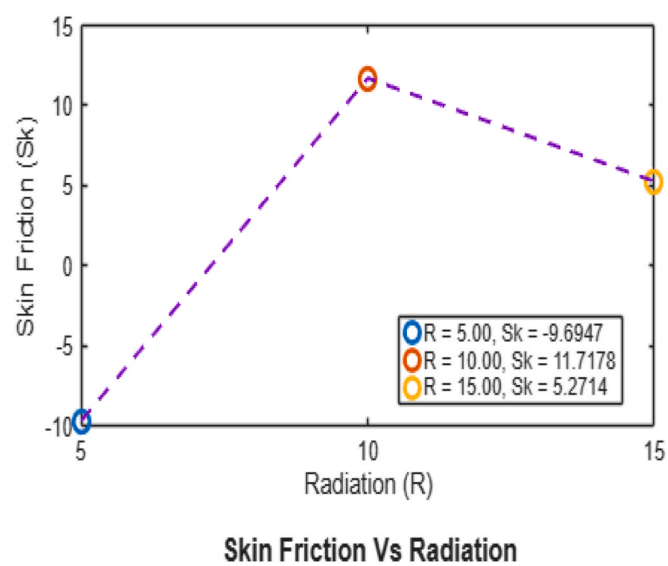

Fig. 29. Skin friction graph for distinct values of radiation.

Dufour number. Fig. 27 shows that when the Casson parameter (γ) increases, skin friction also increases. A higher γ causes the Casson fluid's non-Newtonian yield stress to decrease, making the fluid behave more like a Newtonian fluid. From Fig. 28, it can be shown that the skin friction coefficient (Sk) increases with increasing mass Grashof number (Gc).With Gc increasing from 5 to 15,Sk decreases from -9.6947 to -0.0899,indicating a reduction in wall shear stress.This behaviour is linked to the increase of the buoyant forces due to the effects of mass diffusion. This increases the velocity close to the plate and decreases flow resistance, which eventually raises the wall shear stress (skin friction). Skin friction diminishes as the radiation parameter (R) increases, as seen in Fig. 29. Increased thermal radiation lowers the fluid's temperature and inhibits buoyancy-driven flow by increasing energy loss from the fluid. The skin friction coefficient (Sk) lowers dramatically with increasing the Thermal Grashof number (Gr) as can be shown in Fig. 30. The Sk varies from -9.6947 to -51.0173 with increasing Gr from 5 to 15 which indicates the growth of the magnitude of the wall shear stress.This trend indicates that the higher thermal buoyancy forces intensify the fluid velocity differences close to the plate. Skin friction is decreased as a result of a weaker velocity gradient close to the wall. As a result, radiation dampens the Casson fluid's motion. The primary flow velocity is lowered by the stabilising Coriolis force introduced by rotational effects. Skin friction is reduced as a result of this velocity field suppression, which lessens the momentum conveyance towards the wall. As a result, rotation considerably reduces the boundary-layer motion. As the Prandtl number (Pr) rises, skin friction falls, as shown in Fig. 31. Lower thermal diffusivity, which lowers the temperature boundary-layer thickness and diminishes thermal buoyancy forces, is correlated with higher Pr. The fluid velocity close to the wall reduces as buoyancy does, resulting in a smaller velocity gradient and less skin friction. Consequently, there is less shear stress at the surface of fluids with high Prandtl values (see Fig. 30) (see Fig. 28).

The results are indeed comparable to the previously presented data, as illustrated in Tables 1–3. The analysis was conducted with both accuracy and authenticity. Table 1 shows that the Nusselt number (Nu) is significantly affected by radiation (R), time (t) and the Prandtl number (Pr), which might seem to hinder heat transport, but they actually help it. Table 2 demonstrates that the chemical reaction parameter (K), the Schmidt number(Sc), and time (t) significantly influence the Sherwood number (Sh). This illustrates how these factors alter the mechanisms of mass transfer. Table 3 illustrates that the skin friction coefficient (τ) increases with rising temperature, solutal Grashof numbers (Gr, Gc), inclination angle (α), and the Dufour number. This suggests that buoyant

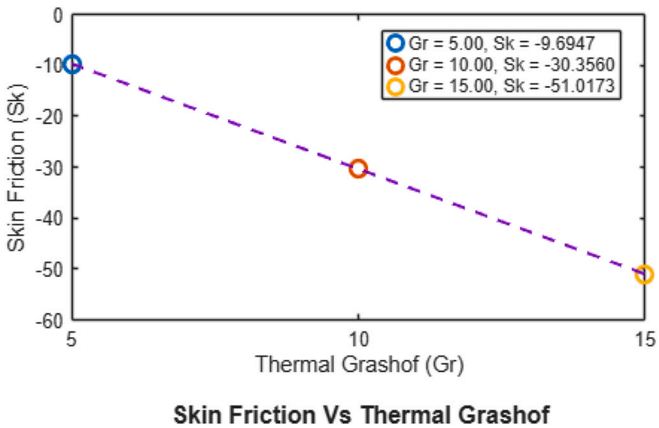

Fig. 30. Skin friction graph for distinct values of Thermal Grashof.

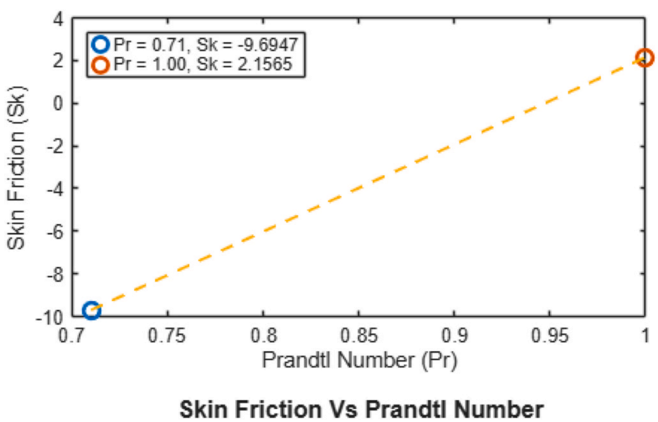

Fig. 31. Skin friction graph for distinct values of Prandtl Number.

forces are crucial.

Practical Implications: The present study has direct practical relevance in processes involving non-Newtonian conducting fluids such as polymer melts, blood flow, food slurries, and industrial pastes. The influence of the Hall current is significant in electromagnetic pumps, MHD generators, and metallurgical processing, where strong magnetic fields are applied. The Dufour effect becomes important in systems involving simultaneous heat and mass transfer, such as drying technology, chemical reactors, and food dehydration processes. Radiation-assisted heat generation is relevant in high-temperature manufacturing, solar energy systems, and thermal processing units. The rotational effects are applicable in rotating machinery, turbines, rotating reactors, and geophysical flows. Understanding the variation of skin friction, Nusselt number, and Sherwood number helps in optimizing surface drag, heat transfer rate, and mass transfer efficiency, thereby improving industrial design, cooling systems, and material processing applications.

Table 1
Nusselt number Nu.

R	Pr	t	Nu (Present Study)	Nu (Literature Value)	Author	
2.0	0.71	**0.4**	−1.8214	−0.8053	U.S. Rajput, G.	**R**
3.0	0.71	**0.4**	−2.1066	−0.8940	Kumar (2017)	
4.0	0.71	**0.4**	5.9616	−0.9761		
2.0	**1.0**	**0.4**	−3.6076	−1.9593	U.S. Rajput, G. Kumar (2017)	**Pr**

Table 2
Sherwood number Sh.

K	Sc	t	Sh (Present Study)	Sh (Literature Value)	Author	
1.0	2.01	0.2	1.0636	−0.7662	U.S. Rajput,	**K**
5.0	2.01	0.2	1.4301	−0.9330	Gaurav Kumar	
10.0	2.01	0.2	1.8089	−1.1182	(2017)	
1.0	**3.0**	0.2	1.2994	−0.9311	U.S. Rajput,	**Sc**
1.0	**4.0**	0.2	1.5004	−1.0752	Gaurav Kumar (2017)	

Table 3
Skin Friction τ

Gr	Gc	df	β	Pr	R	Q	t	*Sk*
5	5	1	0.10	0.71	5.0	1.0	0.2	−9.6947
10	5	1	0.10	0.71	5.0	1.0	0.2	−30.3559
15	5	1	0.10	0.71	5.0	1.0	0.2	−51.0173
5	**5**	1	0.10	0.71	5.0	1.0	0.2	−9.6947
5	**10**	1	0.10	0.71	5.0	1.0	0.2	−4.8923
5	**15**	1	0.10	0.71	5.0	1.0	0.2	−0.0899
5	5	**1**	0.10	0.71	5.0	1.0	0.2	−9.6947
5	5	**2**	0.10	0.71	5.0	1.0	0.2	−1.1907
5	5	**3**	0.10	0.71	5.0	1.0	0.2	3.6617
5	5	1	**0.10**	0.71	5.0	1.0	0.2	−9.6947
5	5	1	**0.20**	0.71	5.0	1.0	0.2	−19.9056
5	5	1	**0.30**	0.71	5.0	1.0	0.2	−31.2871
5	5	1	0.10	**0.71**	5.0	1.0	0.2	−9.6947
5	5	1	0.10	**1.0**	5.0	1.0	0.2	2.1565
5	5	1	0.10	0.71	**5.0**	1.0	0.2	−9.6947
5	5	1	0.10	0.71	**10.0**	1.0	0.2	11.7178
5	5	1	0.10	0.71	**15.0**	1.0	0.2	5.2714
5	5	1	0.10	0.71	5.0	**1.0**	0.2	−9.6947
5	5	1	0.10	0.71	5.0	**2.0**	0.2	−31.4805
5	5	1	0.10	0.71	5.0	**3.0**	0.2	−53.2663

5. Conclusion

This study presents an analytical investigation of Casson fluid flow over an inclined, exponentially accelerating, heated permeable plate under the combined effects of Hall current, Dufour effect, radiation-assisted heat generation, and rotation. The results reveal that fluid velocity increases with the enhancement of heat generation, Hall current, Dufour number, inclination angle, and Casson parameter, whereas it decreases with increasing radiation and rotational effects due to energy loss and Coriolis forces.

The thermal behaviour indicates that temperature rises with Dufour effect and internal heat generation, while radiation reduces the temperature distribution, demonstrating the competing mechanisms of heat transfer. Additionally, concentration decreases with increasing chemical reaction parameter, highlighting the role of reaction kinetics in mass transfer processes. The analysis of skin friction (τ), Nusselt number (Nu), and Sherwood number (Sh) shows that transport characteristics are significantly influenced by the governing physical parameters.

The research confirms that the properties of non-Newtonian Casson fluid significantly enhance flow velocity by reducing yield stress effects.

The plate's exponential acceleration has a major effect on the transient flow, which makes the velocity and thermal boundary layers develop quickly.

The change in skin friction (τ) reveals that surface drag is particularly sensitive to the Dufour effect, the heat source, and the Casson parameter.

A porous material slows down the flow of fluids because it lets them pass through it. This shows how it influences how fluids move. Because the gravitational force along the surface is stronger, an inclined plate speeds up the flow of heat and enhances the transmission of heat.

5.1. Future scope

The model can be extended to turbulent flow, variable thermophysical properties, and different geometries such as cylinders, channels, and stretching surfaces.

Further enhancement can include nanofluids, slip boundary conditions, and non-linear radiation effects for improved heat transfer analysis.

Future work may involve experimental or CFD validation and extension to time-dependent and three-dimensional flow models.

5.2. Limitations of the study

The analysis is limited to laminar, incompressible flow over an idealized plate, neglecting turbulence, slip effects, and variable fluid properties.

Nomenclature

B_0 – Applied Magnetic field (T)	t – Dimensionless time
C – Dimensionless Concentration	t^* – Time (s)
C^* – Species concentration in the fluid (mol/m^3)	u_0 – Velocity of the plate
C_p – Specific heat at constant pressure (J/Kg. K)	$(u^*\ v^*\ w^*)$ – Components of Velocity Field F. (m/s)
C_w^* – Concentration of the plate	$(u\ v\ w)$ – Non-Dimensional Velocity Components
C_∞^* – Concentration of the fluid far away from the plate	$(x^*\ y^*\ z^*)$ – Cartesian Co-ordinate
D – Mass diffusion coefficient	z – Non-dimensional coordinate normal to the plate
$erfc$ – error complementary function	K_1 – Magnetic Permeability (H/m)
Gc – Mass Grashof number	υ – Kinematic Viscosity (m^2/s)
Gr – Thermal Grashof number	Ω^* – Component of Angular Velocity (rad/s)
g – Acceleration due to gravity	Ω – Non -Dimensional Angular Velocity
k – Chemical Reaction Parameter(W/m. K)	ρ – Fluid Density (kg/m^3)
M – Hartmann number	σ – Electric Conductivity (Siemens/m)
Pr – Prandtl number	θ – Dimensionless temperature
Sc – Schmidt number	η – Similarity parameter
T^* – Temperature of the fluid near the plate (K)	β – Volumetric coefficient of thermal expansion
T_w^* – Temperature of the plate (K)	β^* – Volumetric coefficient of expansion with concentration
T_∞^* – Temperature of the fluid far away From the plate (K)	α – Angle of inclination
ω – Rotation parameter	γ – Non-dimensional Casson fluid Parameter
hc – Hall current parameter	
Q – Heat source parameter	

CRediT authorship contribution statement

S. Abirami: Data curation, Resources, Software. **A. Selvaraj:** Methodology, Project administration, Supervision. **A. Kavitha:** Writing – original draft. **D. Lakshmikaanth:** Software. **G. Kuppuswami:** Writing – review & editing.

Declaration of competing interest

The authors declare that they have no known competing financial interests or personal relationships that could have appeared to influence the work reported in this paper.

References

[1] M.S. Abel, N. Mahesha, Effects of thermal buoyancy and variable thermal conductivity in a power law fluid past a vertical stretching sheet in the presence of non-uniform heat source-international, Journal of Nonlinear Mechanics 44 (2009) 1–12.

[2] Utpal Jyoti Das, MHD mixed convective slip flow of casson fluid over a porous inclined plate with Joule heating, viscous dissipation and thermal radiation, J. Math. Comput. Sci. (2021), https://doi.org/10.28919/jmcs/5713.

[3] M.S. Alam, M.M. Rahman, M.A. Samad, Dufour and soret effects on unsteady MHD free convection and mass transfer flow past a vertical porous plate in a porous medium, Nonlinear Anal. Model Control 11 (3) (September 1, 2006) 217–226, https://doi.org/10.15388/na.2006.11.3.14743.

[4] M.S. Alam, M.M. Rahman, Dufour and soret effects on mixed convection flow past a vertical porous flat plate with variable suction, Nonlinear Anal. Model Control 11 (1) (February 27, 2006) 3–12, https://doi.org/10.15388/na.2006.11.1.14761.

[5] M.S. Alam, M.M. Rahman, M.A. Samad, Numerical study of the combined free-forced convection and mass transfer flow past a vertical porous plate in a porous medium with heat generation and thermal diffusion, Nonlinear Anal. Model Control 11 (4) (November 1, 2006) 331–343, https://doi.org/10.15388/na.2006.11.4.14737.

[6] Radha Ganesan, Ayothi Selvaraj, Soundararajan Bhavani, Periasamy Selvaraju, Magneto hydrodynamic effects on unsteady free convection casson fluid flow past on parabolic accelerated vertical plate with thermal diffusion, J. Adv. Res. Fluid Mech. Therm. Sci. 116 (1) (April 25, 2024) 184–200, https://doi.org/10.37934/arfmts.116.1.184200.

[7] S. Dilip Jose, A. Selvaraj, Convective, heat and mass transfer effects of rotation on parabolic flow past an accelerated isothermal vertical plate in the presence of chemical reaction of first order, JP J. Heat Mass Transf. 24 (1) (2021) 191–206, https://doi.org/10.17654/HM024010191.

[8] E. Jothi, A. Selvaraj, Dufour effect on MHD flow past an exponentially accelerated vertical plate through porous system with variable temperature and mass diffusion J, Math. Comput. Sci. 11 (5) (2021) 6205–6215, https://doi.org/10.28919/jmcs/6104.

[9] A. Selvaraj, E. Jothi, Heat source impact on MHD and radiation absorption fluid flow past an exponentially accelerated vertical plate with exponentially variable temperature and mass diffusion through a porous medium, Mater. Today Proc. 46 (2021) 3490–3494, https://doi.org/10.1016/j.matpr.2020.11.919.

[10] S. Karthikeyan, A. Selvaraj, M. Venkateswarlu, Rotating significance of parabolical movement Antique with an appearance on isothermal vertical plate by MHD, Mater. Today Proc. 51 (2022) 1120–1123, https://doi.org/10.1016/j.matpr.2021.07.109.

[11] S. Karthikeyan, A. Selvaraj, Uniform mass diffusion on thermal radiation with rotation of parabolic in progress vertical plate set MHD, Mater. Today Proc. 51 (2022) 1074–1078, https://doi.org/10.1016/j.matpr.2021.07.098.

[12] S. Kavitha, A. Selvaraj, S. Senthamilselvi, P. Rajesh, A parabolic flow with MHD, the dufour and rotational effects of uniform temperature and mass diffusion through an accelerating vertical plate in the presence of chemical reaction, J. Adv. Res. Fluid Mech. Therm. Sci. 110 (2) (2023) 192–205.

[13] Himangshu Kumar, Rudra Kanta Deka, "Thermal and Mass Stratification Effects on Unsteady Flow Past an Accelerated Infinite Vertical Plate with Variable Temperature and Exponential Mass Diffusion in Porous Medium.", East Eur. J. Phys. (4) (December 2, 2023) 87–97, https://doi.org/10.26565/2312-4334-2023-4-09.

[14] G. Aruna, S. Vijayakumar Varma, R. Srinivasa Raju, Combined influence of Soret and Dufour effects on unsteady hydromagnetic mixed convective flow in an accelerated vertical wavy plate through a porous medium.", Int. J. Adv. Appl. Math. Mech. 3 (1) (2015) 122–134.

[15] K. Balamurugan, M. Selvarasu, V. Gopikrishnan, MHD free convection flow past a vertical porous plate in a slip flow regime with radiation chemical reaction and temperature gradient dependent heat source in presence of dufour effect, Malaya J. Matematik 9 (1) (2021) 631–638, https://doi.org/10.26637/mjm0901/0109.

[16] V. Manjula, K. Venkata Chandra Sekhar, Radiation and mass transfer effects on MHD flow of Casson fluid past an impulsively started Isothermal vertical plate, in: 2nd International Conference on Advanced Information Scientific Development (ICAISD) 2021: Innovating Scientific Learning for Deep Communication, vol.2714, 2023 030002, https://doi.org/10.1063/5.0143116.

[17] Richa Deb Dowerah, Nazibuddin Ahmed, Hiren Deka, Radiation absorption effect on MHD natural convective flow past an impulsively started infinite vertical plate with chemical reaction and thermal radiation, Heat Transfer 53 (6) (April 11, 2024) 2689–2711, https://doi.org/10.1002/htj.23057.

[18] Bijjula Prabhakar Ready "Thermo-diffusion and Hall effects on radiating and reacting MHD convective heat absorbing fluid past an exponentially accelerated vertical porous plate with ramped temperature." J. Serb. Soc. Comput. Mech., vol.14, No.1, pp.12-,https://doi:10.24874/jsscm.2020.14.01.02.

[19] Bijjula prabhakar ready and oluwole D makinde "Numerical study on MHD radiating and reacting unsteady slip flow past a vertical permeable plate in a porous medium", Int. J. Ambient Energy,https://doi:10.1080/01430750.2021.1999323.

[20] Bijjula prabhakar ready and oluwole D makinde "Radiating and reacting unsteady MHD free Convection boundary layer flow past an oscillating vertical plate in a porous medium with Newtonian heating." Int. J. Appl. Mech. Eng., vol. 27, No.1, pp.168-187, https://doi:10.2478/ijame-2022-0011.

[21] Prabhakar Reddy B, Simba M. H, and Alfred Hugo "Effects of thermo-diffusion and chemical reaction on MHD radiated unsteady flow past an exponentially accelerated inclined permeable plate embedded in a porous medium. "Int. J. Chem. Eng., https://doi.org/10.1155/2023/9342174.

[22] Ching-Yang Cheng, Soret and dufour effects on free convection boundary layer over a vertical cylinder in a saturated porous medium, Int. Commun. Heat Mass Tran. 37 (7) (August 2010) 796–800.

[23] Ching-Yang Cheng, Soret and dufour effects on free convection boundary layers of non-newtonian power law fluids with yield stress in porous media over a vertical

plate with variable Wall heat and mass fluxes, Int. Commun. Heat Mass Tran. 38 (5) (May 2011) 615–619.

[24] Ching-Yang Cheng, Soret and dufour effects on free convection heat and mass transfer from an arbitrarily inclined plate in a porous medium with constant Wall temperature and concentration, Int. Commun. Heat Mass Tran. 39 (1) (January 2012) 72–77, https://doi.org/10.1016/j.icheatmasstransfer.2011.09.003.

[25] D. Chenna Kesavaiah, R.S. Jahagirdar, Radiation absorption and chemical reaction effects on MHD flow through porous medium past an exponentially accelerated inclined plate, Int. J. Res. Appl. Sci. Eng. Technol. 6 (6) (Jun 30, 2018) 1370–1381, https://doi.org/10.22214/ijraset.2018.6199.

[26] D. Chenna Kesavaiah, P.V. Satyanarayana, MHD and diffusion thermo effects on flow accelerated vertical plate with chemical reaction, Indian J. Appl. Res. 3 (7) (2013) 310–314, https://doi.org/10.15373/2249555x/july2013/96.

[27] Chinmoy Rath, Anita Nayak, Satyananda Panda, Impact of viscous dissipation and Dufour on MHD natural convective flow past an accelerated vertical plate with Hall current, Heat Tran. Asian Res. (2022), https://doi.org/10.1002/htj.22577 first published on May 9.

[28] R. Hetnarski, On inverting the Laplace transforms connected with the error function, Appl. Math. 4 (7) (1964) 399–405, 10.4064/am-7-4-399-405.

[29] Richard B. Hetnarski, An algorithm for generating some inverse Laplace transforms of exponential form, Zeitschrift für angewandte Mathematik und Physik ZAMP 26 (1975) 249–253, https://doi.org/10.1007/bf01591514.

[30] D. Lakshmikaanth, A. Selvaraj, P. Selvaraju, S. Dilip Jose, Hall and heat source effects of flow past a parabolic accelerated isothermal vertical plate in the presence of chemical reaction and radiation, JP J. Heat Mass Transf. 34 (2023) 105–126, https://doi.org/10.17654/0973576323035, 3.

[31] D. Lakshmikaanth, A. Selvaraj, S. Bhavani, Exploration of the impacts of hall effect, dufour effect, and heat source on parabolic flow over an infinite vertical plate in the presence of rotation, chemical reaction, and radiation in a porous medium, CFD Lett. 17 (1) (2025) 60–77, https://doi.org/10.37934/cfdl.17.1.6077.

[32] N. Ameer Ahammad, M. Veera Krishna, Ebrahem A. Algehyne, Heat and mass transfer on unsteady MHD flow of Casson fluid over an infinite perpendicular absorbent plate with slip effects, Heat Transfer 51 (7) (May 31, 2022) 6685–6704, https://doi.org/10.1002/htj.22618.

[33] K.V.B. Rajakumar, K.S. Balamurugan, M. Umasankara Reddy, Ch V. Ramana Murthy, Radiation, dissipation and dufour effects on MHD free convection casson fluid flow through a vertical oscillatory porous plate with ion-slip Current, Int. J. Heat Technol. 36 (2) (June 30, 2018) 494–508, https://doi.org/10.18280/ijht.360214.

[34] V.B. Raja Kumar K, K.S. Balamurugan, Ch V. Ramana Murthy, N. Ranganath, Viscous dissipation and dufour effects on MHD free convection flow through an oscillatory inclined porous plate with hall and ion-slip Current, Int. J. Eng. Technol. 7 (4.5) (September 22, 2018) 410, https://doi.org/10.14419/ijet.v7i4.5.20194.

[35] Kumar, M. Anil, Y. Dharmendar Reddy, B. Shankar Goud, V. Srinivasa Rao, Effects of Soret, dufour, hall Current and rotation on MHD natural convective heat and mass transfer flow past an accelerated vertical plate through a porous medium, Int. J. Thermofluids 9 (February 2021) 100061, https://doi.org/10.1016/j.ijft.2020.100061.

[36] V. Rajesh, S.V.K. Varma, Heat source effects on MHD flow past an exponentially accelerated vertical plate with variable temperature through a porous medium, Int. J. Appl. Math. Mech. 6 (12) (2010) 68–78.

[37] M. Umamaheswar, S.V.K. Varma, M.C. Raju, Unsteady MHD free convective visco-elastic fluid flow bounded by an infinite inclined porous plate in the presence of heat source, viscous dissipation and ohmic heating, Int. J. Adv. Sci. Technol. 61 (December 31, 2013) 39–52, https://doi.org/10.14257/ijast.2013.61.05.

[38] B.V. Swarnalathamma, D.M. Praveen Babu, M. Veera Krishna, Combined impacts of radiation absorption and chemically reacting on MHD free convective Casson fluid flow past an infinite vertical inclined porous plate, J. Comput. Math. Data Sci. 5 (2022) 100069, https://doi.org/10.1016/j.jcmds.2022.100069.

[39] Md Yousuf Ali, Mizanur Rahman, Statistical analysis of periodic MHD chemically radiative Casson flow over an inclined cylinder with entropy optimisation, Heliyon 10 (22) (2024) e40021.

[40] M. Chitra, S. Jeevitha, B. Rushi Kumar, Effects of cross diffusion on radiative MHD flow over a rotating cone through porous medium, Numer. Heat Tran., Part B: Fundamentals 86 (3) (2025) 660–678.

[41] Prasun Choudhary, K. Loganathan, Kavita Jat, Kalpna Sharma, S. Eswaramoorthi, Shape factor analysis of water and aluminium oxide nanoparticles in a porous medium with slip effects, Chem. Phys. Impact 10 (2025) 100882, https://doi.org/10.1016/j.chphi.2025.100882.

[42] Prasun Choudhary, Sushila Choudhary, Kavita Jat, K. Loganathan, S. Eswaramoorthi, Impacts of unsteady MHD Hybrid nanofluid over a non-linear stretchable porous sheet with thermal radiation and gyrotatic microorganisms, Int. J. Thermofluids 23 (2024) 100788, https://doi.org/10.1016/j.ijft.2024.100788.

[43] Karuppusamy Loganathan, S. Eswaramoorthi, P. Chinnasamy, Reema Jain, Ramkumar Sivasakthivel, Rifaqat Ali, N. Nithya Devi, Heat and mass transport in Casson Nanofluid flow over a 3-D Riga plate with cattaneo-christov double flux: *a computational modelling through analytical method*, Symmetry 15 (3) (2023) 725, https://doi.org/10.3390/sym15030725.

[44] P. Kavya, K. Loganathan, K. Chellapriya, S. Eswaramoorthi, S. Divya, Krishna Prakash Arunachalam, P. Senthilkumar, Forecasting of heat and mass transfer in Casson Nanofluid flow with entropy optimisation: machine learning approach, Discov. Appl. Sci. 7 (2025) 747, https://doi.org/10.1007/s42452-025-07364-9.

[45] Sademaki, L. Joseph, B. Prabhakar Reddy, P.M. Matao, Cross-Diffusion process for degradation of methylene Blue by Unsteady MHD Casson natural heat-driven nanofluid flow via an absorbent vertical heated cone in a porous membrane, J. Therm. Anal. Calorim. 150 (online) (2025), https://doi.org/10.1007/s10973-025-14251-3.

[46] Sademaki, L. Joseph, B. Prabhakar Reddy, P.M. Matao, Computational analysis of radiation-absorptive unsteady magnetised thermogenic nanofluid flow with viscous dissipation and chemical reaction from an angled vertical cone in a porous medium, International Journal of Applied and Computational Mathematics (or International Journal of Applied & Computational Mathematics; online) (2025), https://doi.org/10.1007/s40819-025-01929-3.

[47] L. Joseph Sademaki, Md Shamshuddin, B. Prabhakar Reddy, S.O. Salawu, Unsteady Casson hydromagnetic convective porous media flow with reacting species and heat source: Thermo-Diffusion and Diffusion-Thermo of tiny particles, Partial Diff. Equat. Appl. Math. 11 (4) (2024) 100867, https://doi.org/10.1016/j.padiff.2024.100867.

[48] Sademaki, L. Joseph, Md Shamshuddin, S.O. Salawu, B. Prabhakar Reddy, Unsteady dynamical analysis of convective hydromagnetic thermal migration of chemically reacting tiny species with dissipation and radiation in an inclined porous plate, Int. J. Mod. Phys. B 38 (32) (2024) 2450442, https://doi.org/10.1142/S0217979224504423.

[49] Paul M. Matao, Jumanne Mng'ang'a, B. Prabhakar Reddy, Thermal radiation effect on fractional MHD couette flow of Jeffrey Fluid in a vertical channel with activation energy and Joule heating, Partial Diff. Equat. Appl. Math. (2025) 101251, https://doi.org/10.1016/j.padiff.2025.101251.

[50] Sademaki, L. Joseph, B. Prabhakar Reddy, Paul M. Matao, Thermophoresis and brownian motion impact on diffusional heat-generating MHD Jeffrey Nanofluid over an inclined vertical cone with reactive species, Discov. Appl. Sci. 7 (2025) 1136, https://doi.org/10.1007/s42452-025-06840-6.

[51] Sademaki, L. Joseph, B. Prabhakar Reddy, P.M. Matao, Computational analysis of radiation-absorptive unsteady magnetised thermogenic nanofluid flow with viscous dissipation and chemical reaction from an angled vertical cone in a porous medium, Int. J. Algorithm. Comput. Math. (2025), https://doi.org/10.1007/s40819-025-01929-3.

[52] Sademaki, L. Joseph, B. Prabhakar Reddy, Paul M. Matao, A numerical simulation of unsteady dissipative MHD casson nanofluid transport over an inverted cone with variable heat Source/Consumption and high order of reacting species, Multiscale Multidiscip. Multiscale Exp. Des. 8 (5) (2025) 230, https://doi.org/10.1007/s41939-025-00809-z.

[53] N. Casson, A flow equation for pigment–oil suspensions of the printing ink type, in: C.C. Mill (Ed.), Rheology of Disperse Systems, Pergamon Press, London, 1959, pp. 84–102.

[54] Kenneth R. Cramer, Shih-I Pai, Magnetofluid Dynamics for Engineers and Applied Physicists, McGraw-Hill, New York, 1973.

[55] George W. Sutton, Sherman Arthur, Engineering Magnetohydrodynamics, McGraw-Hill, New York, 1965.

[56] H.P. Greenspan, The Theory of Rotating Fluids, Cambridge University Press, Cambridge, 1968.

[57] Svein Rosseland, Theoretical Astrophysics, Clarendon Press, Oxford, 1936.

[58] M. Quentin Brewster, Thermal Radiative Transfer and Properties, Wiley, New York, 1992.

[59] Ernst R.G. Eckert, Robert M. Drake Jr., Analysis of Heat and Mass Transfer, McGraw-Hill, New York, 1972.

[60] Donald A. Nield, Adrian Bejan, Convection in Porous Media, fifth ed., Springer, New York, 2017.

[61] D. Krishnakanth, P. Lakshminarayana, Influence of Lorentz force and thermal radiation on darcy-forchheimer ternary Hybrid Nanofluid flow around a vertical stretching cylinder, World J. Eng. (2026), https://doi.org/10.1108/WJE-08-2025-0528 ahead-of-print.

[62] D. Krishnakanth, P. Lakshminarayana, Induced magnetic field effect on carreau Nanofluid flow and heat transfer around a stretching cylinder: a comparative analysis, Discov. Nano 21 (1) (February 9, 2026), https://doi.org/10.1186/s11671-026-04430-y.

[63] D. Krishnakanth, P. Lakshminarayana, Influence of thermal diffusion and molecular motion on heat transfer and fluid flow of carreau ternary hybrid nanofluid, Mod. Phys. Lett. B 40 (7) (2026) 2650028, https://doi.org/10.1142/S0217984926500284.

[64] M. Vinodkumar Reddy, P. Lakshminarayana, MHD radiative flow of Williamson Nanofluid with cattaneo–christov model over a stretching sheet through a porous medium in the presence of chemical reaction and Suction/Injection, J. Porous Media 25 (12) (2022) 1–15, https://doi.org/10.1615/JPorMedia.2022041423.

[65] A.B. Sadiya, G. Sucharitha, Computational analysis of MHD Ternary Hybrid nanofluid flow with thermochemical reactions through a porous medium on a rotating stretching sheet, Discov. Nano 20 (1) (September 25, 2025), https://doi.org/10.1186/s11671-025-04353-0.

[66] A.B. Sadiya, G. Sucharitha, Thermal analysis of ternary hybrid nanofluid flow through a porous medium on a rotating stretching sheet with dual stratification effects, World J. Eng. (2025), https://doi.org/10.1108/WJE-05-2025-0343 ahead-of-print.

[67] M. Ajithkumar, P. Lakshminarayana, K. Vajravelu, Diffusion effects on mixed convective peristaltic flow of a Bi-Viscous Bingham Nanofluid through a porous medium with convective boundary conditions, Phys. Fluids 35 (3) (2023) 032008, https://doi.org/10.1063/5.0142003.

[68] Kenneth R. Cramer, Shih-I Pai, Magnetofluid Dynamics for Engineers and Applied Physicists, McGraw-Hill, New York, 1973.

[69] George W. Sutton, Arthur Sherman. Engineering Magnetohydrodynamics, McGraw-Hill, New York, 1965.

[70] Adrian Bejan, Convection Heat Transfer, fourth ed., Wiley, Hoboken, NJ, 2013.

[71] Frank P. Incropera, David P. DeWitt, Theodore L. Bergman, Adrienne S. Lavine, Fundamentals of Heat and Mass Transfer, seventh ed., Wiley, Hoboken, NJ, 2011.
[72] R. Byron Bird, Warren E. Stewart, Edwin N. Lightfoot, Transport Phenomena, second ed., Wiley, New York, 2002.
[73] Hermann Schlichting, Klaus Gersten, Boundary-Layer Theory, ninth ed., Springer, Berlin, 2017.
[74] Michael F. Modest, Radiative Heat Transfer, third ed., Academic Press, Burlington, MA, 2013.
[75] Robert Siegel, John R. Howell, Thermal Radiation Heat Transfer, fifth ed., CRC Press, Boca Raton, 2010.
[76] U.S. Rajput, Gaurav Kumar, Effects of radiation and chemical reaction on MHD flow past an exponentially accelerated inclined plate with variable temperature and mass diffusion in the presence of Hall Current, J. Sci. Arts 17 (3) (2017) 565–572, 40.
[77] Ilango Ms, Lakshminarayana Pallavarapu, Melting heat transfer and entropy analysis of MHD Casson nanofluid flow through a stretchy surface with Joule heating and complete slip, World J. Eng. 22 (5) (2025) 940–951, https://doi.org/10.1108/WJE-01-2024-0016.
[78] M.S. Ilango, P. Lakshminarayana, Induced magnetic field and Soret–Dufour effects on viscous dissipative Casson fluid flow through porous medium over a stretching sheet, J. Therm. Anal. Calorim. 149 (15) (2024) 8713–8727, https://doi.org/10.1007/s10973-024-13352-9.